ABSTRACT

STANTON, BRANDON MATTHEW. Characterization of Vertical Cavity Surface Emitting Lasers with Electrical and Optical Derivative Spectroscopy. (Under the direction of Robert Kolbas.)

The motivation behind this work is to use derivative spectroscopy to better understand the inner workings of Vertical Cavity Surface Emitting Lasers (VCSELs) provided by Honeywell Inc. Derivative spectroscopy was used to investigate two types of Honeywell VCSELs, Oxide confined VCSELs and Proton bombarded VCSELs. To quantify the devices I-V (current-voltage) and P-I (power-current) electrical and optical measurements were used to show the devices have no major problems and that the measurements are reproducible.

The I-V and P-I curves were taken to initially characterize devices. Having these curves supplies basic information such as laser threshold and data points for the slope of the operating regime. Using a voltage modulation technique derivative measurements dI/dV, d^2IdV^2, dL/dV were obtained and revealed subtle nonlinearities in the I-V and P-V data. Near field images of the optical output was correlated with the electrical measurements, and three mechanisms were identified that could be the cause of the derivative structure of the I-V curves.

Characterization of Vertical Cavity Surface Emitting Lasers with Electrical and Optical Derivative Spectroscopy

By
Brandon Matthew Stanton

A thesis submitted to the Graduate Faculty of
North Carolina State University
in partial fulfillment of the
requirements for the Degree of
Master of Science

Electrical Engineering

Raleigh, NC

2003

APPROVED BY:

_____

_____ _____

Personal Biography

Brandon Stanton was born and raised in Durham, NC where he attended Southern Durham High School. At an early age he wanted to be an engineer, so he went on for his Bachelors degree in electrical engineering at North Carolina State University. During his undergraduate course work he found he had an interest in semiconductors and lasers.

Brandon conducted research toward a Masters degree at NC State under the direction of Dr. Robert Kobas. His research involved building test equipment to characterize semiconductor lasers. Brandon plans to complete his graduate research in December 2003. He will be moving to Monterey, California beginning in January 2003 to reunite with his wife Wendy.

TABLE OF CONTENTS

LIST OF TABLES

LIST OF FIGURES

1. Chapter 1 – Introduction

1.1. Motivation

The motivation behind this work is to use derivative spectroscopy to better understand the inner workings of Vertical Cavity Surface Emitting Lasers (VCSELs). VCSELs were invented in the late 1980's[1] but the understanding and characterization of these devices has not yet come to the same level as other semiconductor devices. Semiconductor edge emitting lasers have been researched for the past fourty years and are now very well characterized and understood by using a variety of characterization and modeling tools such as derivative spectroscopy. VCSELs on the other hand are less mature and require further examination to reach the level of understanding that edge emitting lasers have reached.

In an effort to examine VCSELs closer, a cooperative relationship was built between North Carolina State University and Honeywell Inc. Derivative spectroscopy was used to investigate two types of Honeywell VCSELs, Oxide confined VCSELs and Proton bombarded VCSELs. To quantify the devices I-V (current-voltage) and P-I (power-current) electrical and optical measurements were used to show the devices have no major problems and that the measurements are reproducible.

To understand a device as complicated as the VCSEL, measurements other than the standard I-V and P-I curves must be taken. For instance the first derivative of the I-V curve can be used to measure the series resistance that may cause roll-over of the current at high current levels. Second derivative measurements can illuminate a process such as

laser threshold or a mechanism that is parasitic in nature and cause undesired optical patterns or mode shifts. The I-V and P-I curves are where this system of derivatives starts. Having these curves supplies basic information such as laser threshold and data points for the slope of the operating regime. Since voltage is the supplied bias for the diodes rather than current, voltages will be used in explaining diode characteristics such as threshold and where anomalies occur. Using regular P-V curve measurements, the threshold of the oxide devices occur at approximately 1640mV (~2.7mA) which may vary a small amount from diode to diode. The proton devices have a higher threshold approximately 1700mV (~3.5mA).

In this introduction the history and development of derivative spectroscopy is explained along with a short overview of the VCSELs investigated. In the second chapter the experimental setup and procedure used to test the devices is shown and explained. The third chapter includes the measurements/observations and how the measurements were taken with the experimental apparatus. Chapters four and five contain analysis of the observations and measurements. The last chapter consists of a summary, conclusions of analysis, and proposed future work.

1.2. Background on Derivative Spectroscopy

Derivative measurement techniques were first used to detect fine structure in the electrical characteristics of semiconductor devices such as tunnel diodes, transistors, and double heterostructure semiconductor lasers[2]. The measurement systems first created to take derivative measurements used a common technique of ac modulation and harmonic

detection with various circuits. A generic derivative measurement system was developed for derivative measurements with a wide range of testing capabilities in 1971[3]. That system employed circuitry to reject nearly the entire output signal at any fundamental frequency when detecting higher harmonic components of current. These measurements took place throughout the 1970's and made a considerable contribution to the understanding of double heterostructure junction lasers. The advances and implementation of derivative spectroscopy can be found in the literature[4,5,6,7].

1.2.2. Type of Measurement Used for this Experiment

The Quantum Optoelectronics group at North Carolina State University has developed a derivative system based on the same concepts developed in the 1960's and 1970's but implemented with today's integrated circuit technology. Our system works with analog signal processing techniques to provide a low noise environment to recover small signals. The system used to obtain the derivative measurement will be described in detail in Chapter 2.

First derivative measurements are straight forward and are done by superimposing a small ac signal upon a dc bias that is slowly swept through the range of the independent variable. ($V_{applied} = V_{dc} + V_{ac}$) The dc component of the dependent variable is proportional to the response f(x) while the ac component is proportional to the first derivative df(x)/dx shown in Figure 1. While a voltage is applied to the devices, the operating current can be calculated with:

$$I = I_0 e^{V - IR/\eta kT}$$ **Equation 1**

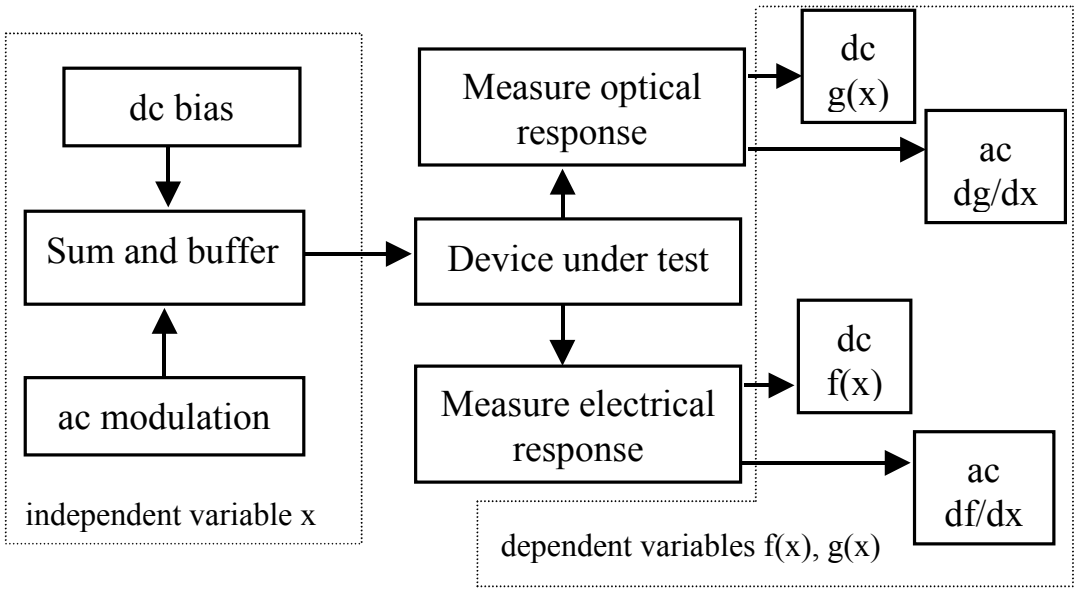

Figure 1 The response to an applied current (voltage) to a device under test results in a response of voltage (current or light output). The first derivative is proportional to magnitude of the ac signal. Improved signal to noise is obtained by using phase sensitive detection to recover the ac signal.

Second derivative measurements are not as simple to obtain. The technique we employ, first suggested by Thomas L. Paoli in 1976[2], makes use of a dual frequency technique for electrically measuring higher order derivatives by frequency mixing. The techniques utilize an ac modulation at two distinct but phase synchronous frequencies to produce derivative signals at a useful difference (or sum) frequency that is unique to the order of the derivative being measured. An example of the two modulation frequencies and the difference frequency used in this system: f_1 = 15kHz, f_2 = 16kHz and $f_2 - f_1$ = 1kHz. The difference frequency, being well away from the modulation frequencies (f_1, f_2) enables better filtering of noise and recovery of the small signal response. This approach is shown schematically in Figure 2. Third order derivatives can be measured by mixing a third frequency, then detecting the difference frequency of the three frequencies used. Theoretically higher order derivatives[8] can also be achieved by mixing nth multiple frequencies and recovering the appropriate sum and difference frequencies.

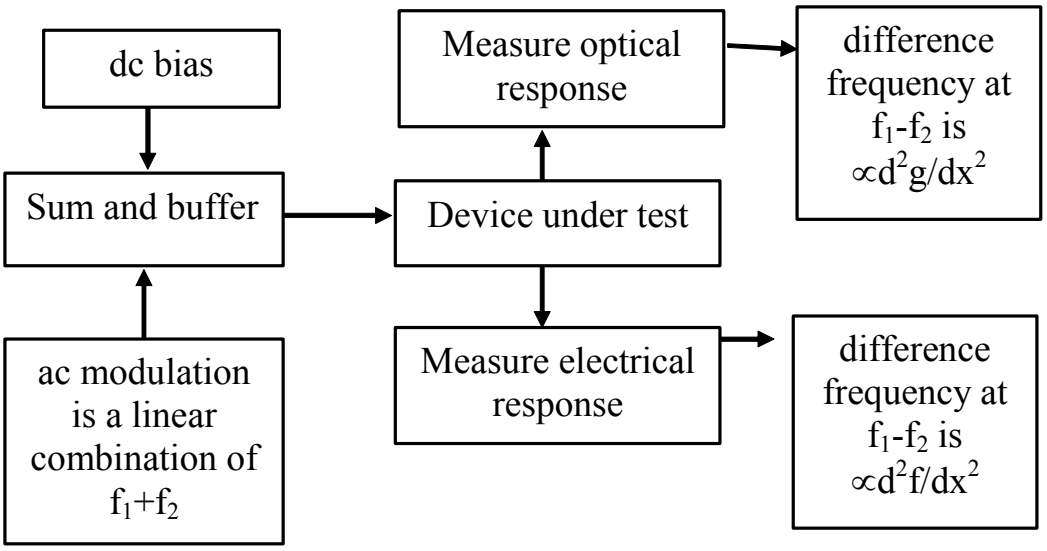

Figure 2 The second derivative is obtained in a low noise environment by using the difference frequency method of Paoli. The generation of a low distortion ac modulation signal in conjunction with time-continuous digitally tunable filters has enable us to construct a derivative system that used analog phase sensitive signal recovery in conjunction with computer control.

Due to the flexibility of this system the light output of the VCSELs being tested were also obtained. Along with the light output from the test device optical derivatives are obtained in the much the same way as the electrical derivatives. A photodiode is used to capture the light output response, as the test device is feed the input signal. The photodiode current is feed through the same type of signal recovery process as the electrical current from the test device. This allows simultaneous light and electrical derivative measurements to be obtained and analyzed together.

Taking the first, second, and sometimes third derivative of the current, voltage or light output from a laser diode identifies more nonlinearities and 'warts' than can be explained by simple single parameter analysis[9,10,11,12]. Significant analysis and interpretation is required because to date there is not a direct correlation between each max, min, null and wiggle in the derivative spectrum to a specific problem or design parameter. These nonlinearities have been thought to come from different optical

processes running in lasers such as multiple filaments lasing in a proton bombarded VCSEL[9]. The correlations between electrical and optical derivatives[13] are better revealed when optical observations are obtained along with the various derivative measurements. Near field measurements of VCSELs have been obtained showing varying optical patterns[14], which with further study will supply the answers needed to show correlations between electrical and optical derivative measurements.

1.3. Background on Vertical Cavity Surface Emitting Lasers

The first surface emitting laser with a vertical cavity was developed in 1979, using a GaInAsP active region, and required a mirror reflectivity of ~85% provided by metallic reflectors. This device worked at liquid nitrogen temperatures and had a large threshold current due to the large active volume[1]. To obtain a room temperature continuous wave VCSEL an AlGaAs / GaAs structure was used to reduce Auger recombination current. The major improvements in VCSEL thresholds were obtain by reducing the active volume of the device. This was done by using quantum wells, which facilitate the reduction of the current threshold density from 44kA/cm^2 down to 1.8kA/cm^2.[15] Even though many improvements have been made since the invention of the VCSEL, using derivative spectroscopy holds promise to further understand and improve these devices.

1.3.2. Band Diagram of a VCSEL

The internal structure of a VCSEL is based on current injection in a P-N junction. A heterostructure is formed by two different materials such as GaAs and AlGaAs coming together to form a quantum well within the p-n junctions. Band diagrams illustrate how a p-n junction and p-n heterojunctions operate under forward bias as shown in Figure 3.

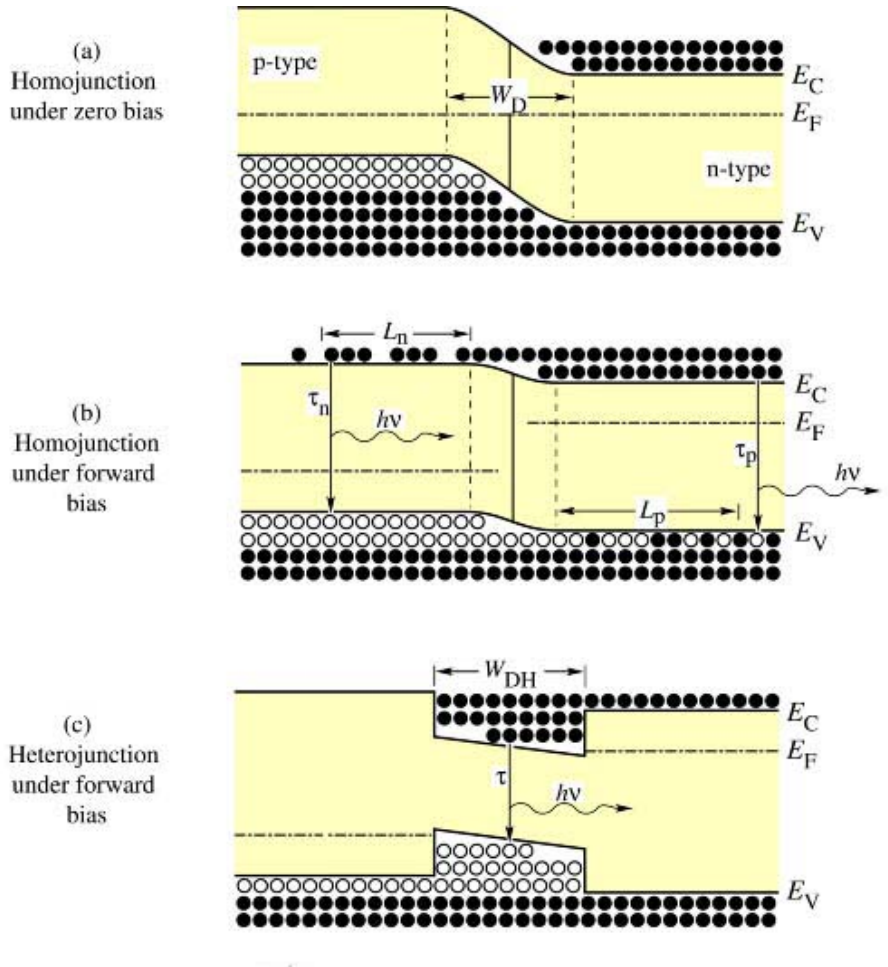

Figure 3 P-N homo and double heterojunctions. The heterojunction improves the confinement of carriers and reduces laser threshold.

1.3.3. VCSEL Structure

In order to have lasing action there are three basic requirements: gain, optical feedback, and external stimulation. This was first achieved in a semiconductor p-n junction in 1962[16]. In these first devices there was electron hole recombination in the p-n junction depletion layer for gain. The laser cavity was formed by cleaved or polished semiconductor surfaces providing the optical feedback, and the p-n junction was forward biased for external stimulation. In 1969 the double heterostructure was introduced, and the edge emitting stripe geometry laser[16] become the standard semiconductor laser configuration. The output of this laser was parallel to the substrate and was not a circle but an ellipse. Many researchers found that a surface emitting structure would better accomplish tasks such as coupling light into optical fiber and making multi-dimensional laser arrays. Before the invention of the VCSEL, many tricks were played with mirrors incorporated in edge emitting lasers to transform them into surface emitting lasers. Then as stated above, the first Vertical Cavity laser was created. The laser cavity is perpendicular to the plane of the active region, rather than parallel as in the edge-emitting laser. This allows for vertical output of the laser light relative to the substrate. The laser cavity is formed with two Distributed Bragg Reflectors (DBRs) with reflectivity R_1 and R_2 positioned opposite one another, a distance L apart.

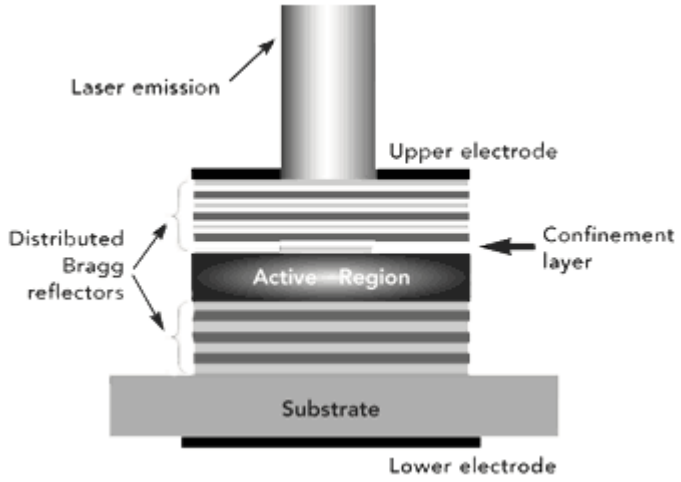

Figure 4 VCSEL Structure

The geometry used for VCSELs was suggested in 1977 for the purpose of overcoming problems such as the initial probe test of devices on wafers, and the integration of lasers into optical circuits due to cavity length restrictions. The VCSEL structure brought about a number of changes. For example, a large numbers of laser devices can be fabricated by a fully monolithic process. The initial probe test can be done on the wafer before dia separation. A narrow circular beam with negligible astigmatism and low beam divergence can be achieved which facilitates fiber coupling and focusing the laser output. Densely packed two dimensional laser arrays could be fabricated and very low threshold operation was obtained[15].

The two VCSEL structures investigated in this document are similar to Figure 4. Both the oxide and proton bombarded VCSELs have two sets of Bragg mirrors and a cavity that will only support one longitudinal Fabry-Perot mode. The main difference between the two structures studied is the method of current confinement; details are provided in chapter 1.3.5. A plan view of the top side of the two chip structures are shown in Figure 5.

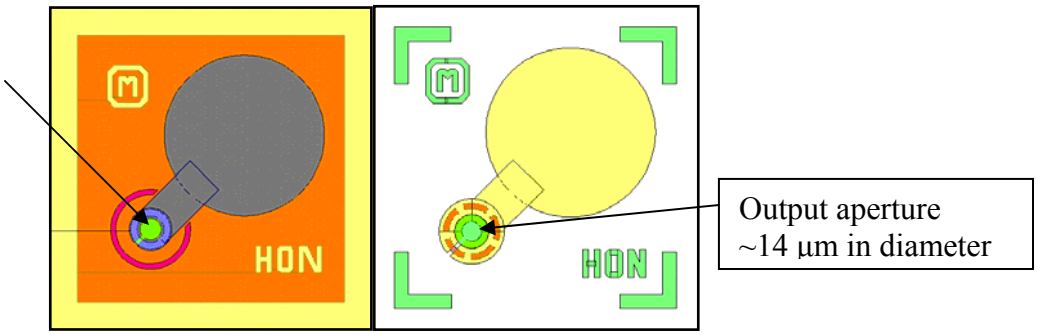

Figure 5 On the left is the Proton VCSEL, where the smaller dot (pointed out by arrows) surrounded by the blue ring is the output aperature. On the right the Oxide VCSEL is shown, the output aperture is also the light green area inside the slotted orange circle.

1.3.4. Current Density Threshold Improvements

The first VCSEL had a large active region volume and low reflectivity metallic mirrors. As stated in a previous section, the J_{th} had been reduced by a factor of more than 500 by reducing the active volume. However, when the active volume was reduced, the total gain was reduced, and a reflectivity larger than the 85% produced by metallic mirrors would be needed. The threshold current density for VCSELs is given by

$$J_{th} = \frac{\alpha_r + \alpha}{\alpha} \frac{ed}{\eta_i \tau_r} \Delta n_T$$

Equation 2[17]

where d = active region thickness, α_r = threshold gain coefficient, α = thermal equilibrium absorption coefficient, τ_r = radiative electron-hole recombination lifetime, η_i = internal quantum efficiency and Δn_T = transparency injected-carrier concentration. To reduce the amount of active volume, a quantum well was introduced to reduce the total volume. The relation of the gain at threshold is given by

$$g_{th} = \alpha + \frac{1}{2L\Gamma} \ln \frac{1}{R_1 R_2}$$

Equation 3

where R_1 and R_2 are the reflectivity of the two mirrors; L is the length of the quantum well; α is the distributed loss coefficient; and Γ is the transverse confinement factor of the optical field in the active layer. Take for example a 100 Å well, g_{th} has a maximum value of 10^3/cm which requires a reflectivity of R > 99% to sustain laser oscillations. Specular metal reflectors are limited to ~.98 by optical absorption within the material. [18,19] The high reflectivity would have to come from a multilayer dielectric material with band gaps higher than that of a material used for the active region. At dielectric interfaces there is a reflection due to the change in refractive indexes as seen in Figure 6. [19] The relation between refractive index of one material to the next for a normal incident plane wave is,

$$R = \frac{(n_1 - n_2)^2}{(n_1 + n_2)^2}$$

Equation 4

This only yields about a 30% reflection with materials such as AlGaAs / GaAs. This alone does not account for the .999 reflectivity that is needed for the gain. To achieve this goal a resonant Bragg multilayer structure is used where the reflection from a number of interfaces may add in phase to produce large reflections given by the following equation.

$$\sqrt{R} = \frac{1 - \frac{n_s}{n_o}\left(\frac{n_1}{n_2}\right)^{2m}}{1 + \frac{n_s}{n_o}\left(\frac{n_1}{n_2}\right)^{2m}}$$ **Equation 5**[19]

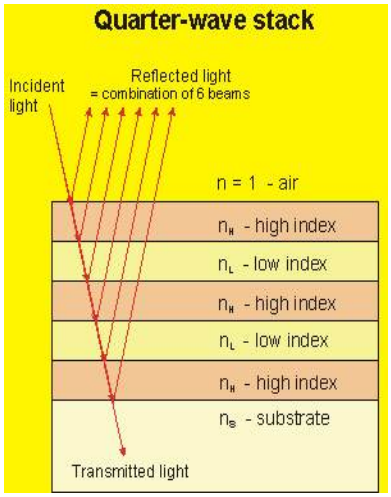

Figure 6 Dielectric mirror stack; at dielectric interfaces there is a reflection due to the change in refractive indexes

The first structure to use these reflectors was a distributed feedback laser developed in 1987[19], which still had a rather large active volume. No significant advances were made until 1989 [18, 19] where high reflectivity dielectric mirrors were used in conjunction with a single quantum well, allowing the J_{th} to be lowered to 1800A/cm^2.

Dielectric stacks are great for DBRs; however the number of layers needed to build up the reflectivity gives these reflectors limitations. The large index of refraction difference between alternating layers is what makes the reflection, however the bandgap difference creates potential barriers to carriers at heterointerfaces resulting in a high resistance device[19]. A typical value for the series resistance in a multimode VCSEL is about 25 ohms and can get as high as 40 ohms. Single mode VCSELs have an even higher series resistance due an increase in layers. In order to work around the problem, a graded heterobarrier can be used in place of the abrupt junction, which reduces the series resistance without sacrificing reflectivity.

1.3.5. Confinement Parameters

Current flows down through the DBRs in order to reach the active region. Without lateral confinement, current spreading will occur as seen in Figure 7. Current injection provides the external stimulation through ohmic contacts on top of the VCSEL as seen in Figure 5. The bond pad and active area are arranged diagonally on the chip. The round bond pad diameter is approximately 120μm for both types of VCSELs investigated.

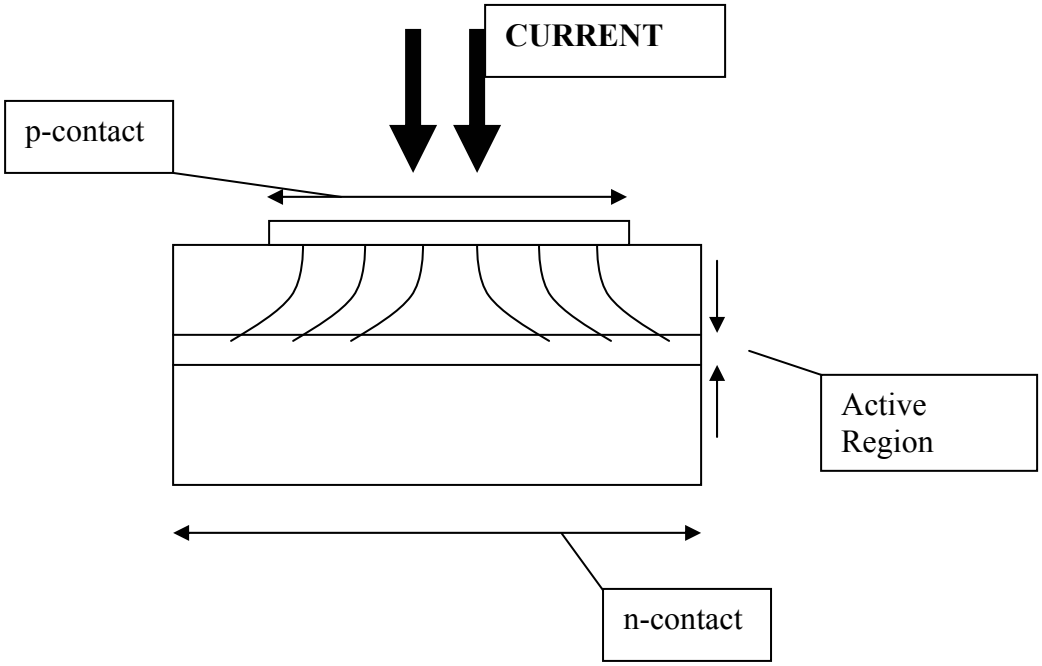

Figure 7 Example of Current Spreading in a device without a current confinement mechanism in place.

Current that is not confined is subject to non-radiative processes such as surface and auger recombination which could lead to reduced performance and device failure. There are a number of methods for achieving the desired current confinement. This section includes two of the methods: oxide confinement and proton implantation.

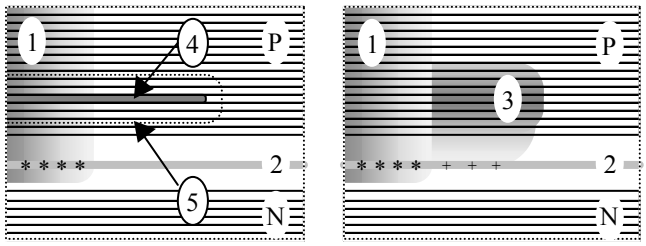

a) Oxide b)Proton

Figure 8 . a) Oxide Confinement left, region 1 represents the multi-energy isolation implant for insulating purposes, region 2 in the figure contains the PN junction (quantum well region), region 4 is the annular ring of aluminum oxide represented by the dark gray stripe, region 5 represents the removal of acceptor concentration in that area; b) Proton Implantation right, region 1 represents the multi-energy isolation implant for insulating purposes, region 3 shown by the dark gray area is the gain-guided proton implant, region 2 in the figure contains the PN junction (quantum well region). Figure from Honeywell International Document [20]

Oxide confined current works more like a dam for water constricting the current flow to a small region through an opening in the dielectric (region 4). In oxide VCSELs the wet thermal oxidation process forms an annular ring of aluminum oxide represented by the dark gray layer (region 4) in Figure 8(a). The oxidation process also removes acceptor concentration from the equivalent of six mirror periods plus the oxide thickness as illustrated by the dotted region (region 5) around the oxide layer in Figure 8(a) [20]. While both methods confine the current, the oxide method also helps to confine the optical mode to the active region better due to an abrupt dielectric interface.

Current confinement is necessary to obtain low J_{th} at room temperature along with other benefits. Restricting the current using the proton implantation scheme creates a region of high resistance that restricts the flow of current to an opening in the implanted region. The depth and range of the gain-guide implant in proton VCSELs is represented by the gray area (region 3) in Figure 8(b). The high lateral sheet resistance below the gain guide gives excellent debiasing of the P-N junction[20] at the isolation implant perimeter [20]. The problem with ion implantation is the damage that occurs when the implanting is

done. If the active region is damaged, defects such as recombination centers may be found creating a significant nkT current under the gain guided implant area [20].

1.4. Objectives of This Work

To make the derivative measurement system work faster and to utilize the speed of the newer computers the plotting and electronic transfer of standard measurements (I-V, dI/dV, d^2I/dV^2, L-V, dL/dV, L-I) is automated. The software needs to be updated to interface with the new computer system. Automating the other programs associated with the data acquisition needs software to process and present the results graphically. In order to visually see what happens to the optical output at each input value the capability to record a single video frame of the VCSEL near field pattern at each value of the independent variable is taken to identify spatial variations across the emitting surface of the device must be added.

2. Chapter 2 – Experimental Setup

2.1. Measurement Devices Used

This chapter contains information about the custom instrument that was designed and built to perform the electrical and optical measurements. Most of the equipment used in this setup was custom built. The main piece of equipment used in this experiment is referred to as the derivative machine. The derivative machine is a multifunctional tool that makes possible various measurements. Associated with the derivative machine are two test fixtures that have specific purposes. A computer program was written to interface the derivative machine for automated data acquisition. The computer and programming language used for the experiments is explained in the following chapter. This chapter explains some of the problems faced when building and updating the measurement system. Updating the system included moving the program to a new Dell desktop computer and installing up to date hardware.

2.1.2. Derivative Machine

The derivative machine consists of a power supply and twelve slots for custom built rack mountable cards to interface with a computer via IEEE 488 GPIB. This machine was built and the circuitry was completed by Dr. Robert Kolbas. The derivative apparatus uses analog modulation and phase sensitive signal recovery of the signals associated with the first and second derivatives. A computer controls the acquisition and

storage of data for later analysis. In Figure 9 a block diagram of the derivative box can be seen. Below is a list of the cards present at this time which make up the electrical derivative system:

- Waveform generator
- Digital to analog converter
- Two current to voltage converters
    - One for electrical feedback from the Laser diode (device under test)
    - One for optical feedback from the Photodiode
- Switch box for routing signals
- Lock-in amplifier
- Analog to digital converter

The function of these plug-in boards and their interaction with the computer is as follows:

1. Waveform generator (wfg) – the computer downloads the appropriate waveform (for first [1kHz] or second derivative [15kHz + 16kHz]) into the wfg which supplies the ac modulation.

2. Digital to analog converter (dac) – receives the ac modulation from the wfg, while also receiving the dc ramp voltage information from the computer, then sums the ac and dc signal to pass through the device.

3. Two low impedance current to voltage converters (cvc) – the cvc's are transimpedance amplifiers that convert a current to a voltage with ($Vout= -R_f I_{in}$) where R_f ranges from 10^6 to 10 ohms in decade steps. The cvc's also perform filtering functions to separate the ac and dc signals.

4. Lock-in amplifier (lock-in) – the ac and dc signals are separated, ac signal is recovered using phase sensitive detection relative to a reference signal (1kHz in this case).

5. Analog to Digital converter (adc) – a voltage signal is digitized by the adc and sent to the computer for storage and later analysis (15 bits + sign).

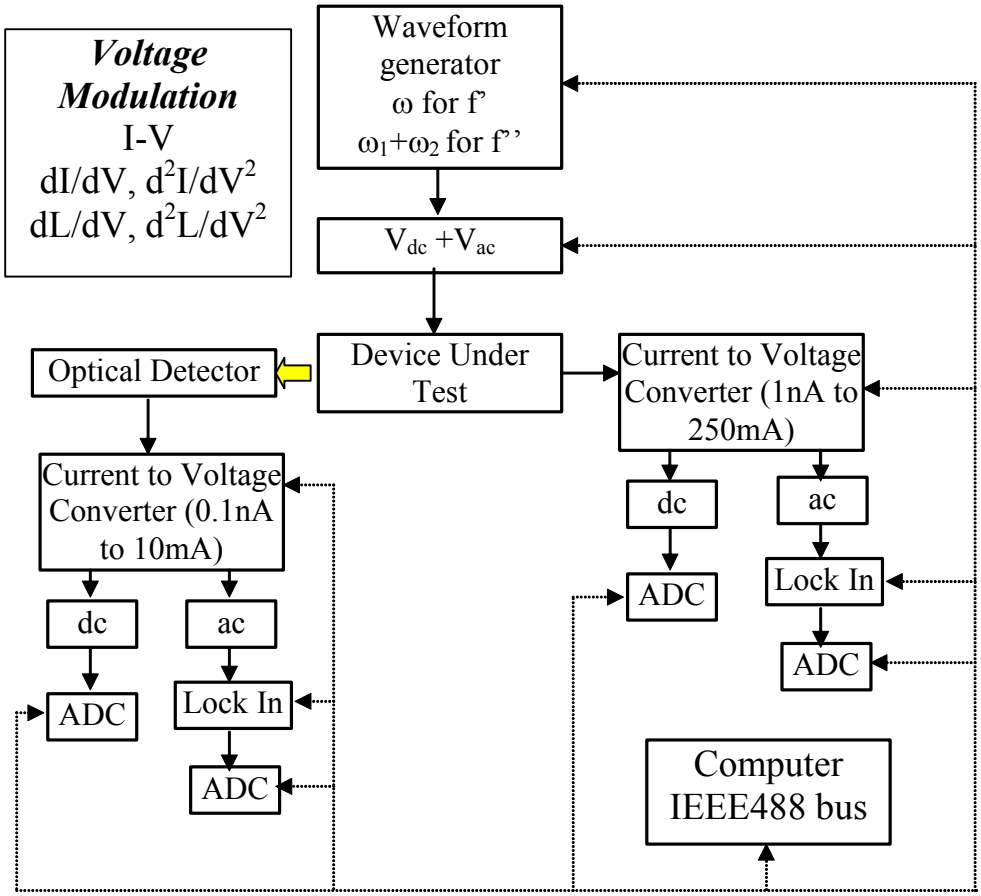

Figure 9 . Functional block diagram of the derivative apparatus. The appropriate waveform for the first or second derivative is downloaded into the programmable waveform generator. The ac modulation is mixed with a dc offset voltage and applied to the device. The resulting current is detected by a low impedance (<1mV offset) current-to-voltage converter. The ac and dc signals are separated, the ac signal is recovered using a lock in amplifier, and then the signals are digitized by analog to digital converters (ADC) and sent to the computer as digital data.

Figure 10 Picture of the derivative machine.

More cards can designed for different purposes. Other DACs can be created with the ability to output a current with modulation. That type of current output DAC card would allow the current to be the independent variable and voltage to be measured as a dependent variable.

To hold the laser diode electrically and capture the light output, various test fixtures were built. There are two test fixtures; the first is the voltage-photodiode fixture and the second is a voltage-camera fixture. Both fixtures use coax cables to connect input and output to the derivative machine as seen in Figure 10.

2.1.3. Voltage Photodiode Test Fixture Setup

The voltage test fixture setup includes two die cast aluminum boxes of differing sizes that contain the laser diode and mounting devices that hold the laser diode. The smaller box is 12cm long, 6.5cm wide and 3.5cm deep. The larger box is 19.5cm long, 11.5cm wide and 5.5cm deep. The larger box has four leg posts with rubber soles for insulating purposes. The smaller box also has four leg posts that are used to elevate the small box inside the larger box. Inside the smaller box a hole was cut into the shorter wall for the connector of a photodiode to be screwed in place. Different photodiodes can be placed inside the box for testing of different wavelengths or low light output. The smaller box is covered with the larger box for extra light containment and to keep ambient light away from the photodiode. The wiring for the photodiode runs through holes in the larger box. The block diagram is shown in Figure 11.

Inside the smaller box is a proto board mounted on four posts, with connection pins sticking upward, to provide electrical and mechanical support to the device under test (laser diode). A holder for the laser diode slides onto the connector pins and holds the laser diode as seen in Figure 12 and Figure 13. Two of the connector pins are wired with coaxial lines for input and output of the laser diode. The output for the laser diode is transferred to a current to voltage converter (cvc) to separate out the Vac and Vdc using band pass filters on the converters. Inside the cvc used for the output from the test device are two filters. One filter is used for the first derivative which is just a high pass filter since the incoming signal is 1 kHz. This filter's output is sent to the lock-in amplifier and then the Analog to Digital converter (adc) to be digitized and stored as numerical data. The second filter contained in this cvc is a band pass filter. This filter is used in conjunction with the second derivative measurements. Since two frequencies are mixed together, the band pass filter can be adjusted to pass the difference frequencies ($f_2 - f_1$).

The photodiode receives light output from the laser diode and the current output from the photodiode is passed via coaxial cables to a second cvc to convert the current and separate the ac and dc signal. At this point the cvc used to separate the Vac and Vdc from the photodiode can not be used in the same way as the cvc used for the test device because this particular cvc does not have a band pass filter to isolate the difference frequencies.

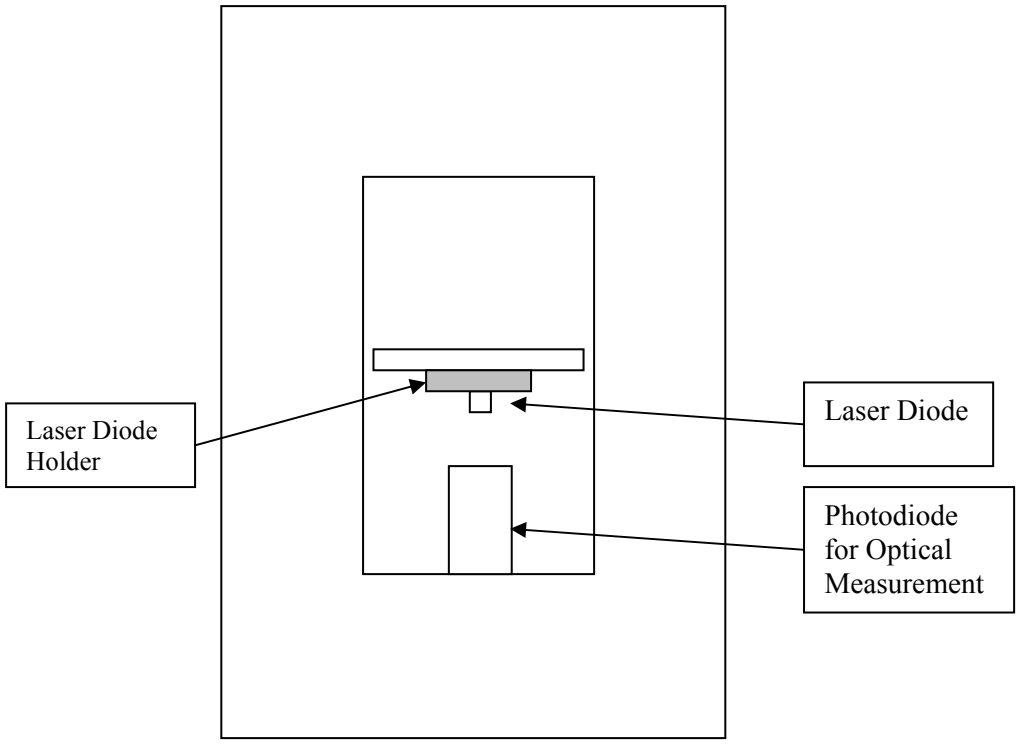

Figure 11 Block diagram of the Voltage Photodiode Test Fixture.

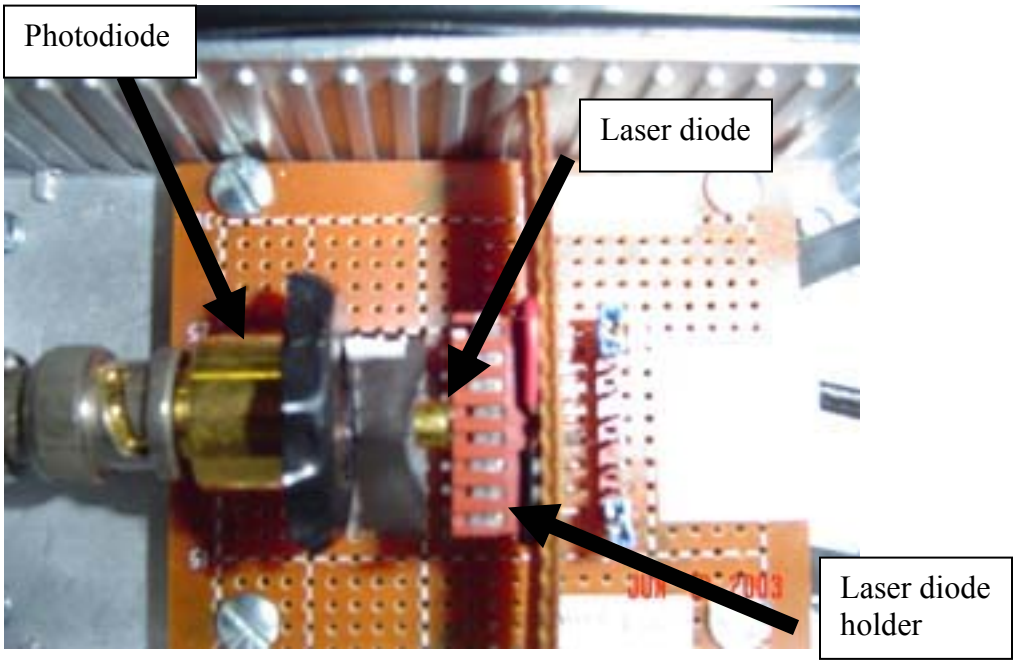

Figure 12 Close up of Laser diode held in front of a photodiode in voltage photodiode box.

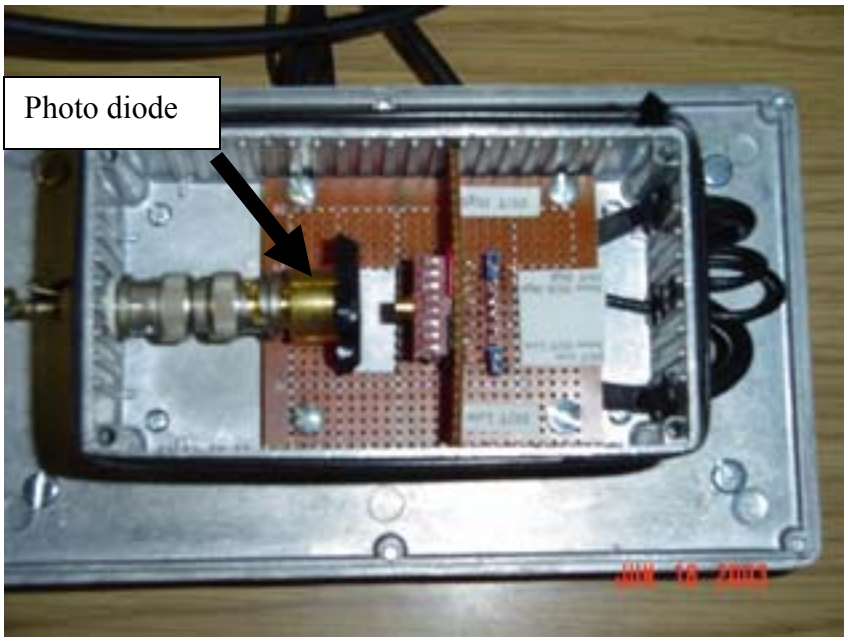

Figure 13 Full view of the Voltage Photodiode test fixture without the inner cover and external light shield removed.

Optical observations must be made in order to better characterize what happens to the optical derivatives. For this reason the test fixture with a camera setup was constructed allowing for the optical mode patterns to be photographed. With the capability of photographing the optical mode patterns, a correlation between modes and voltage/current measurements may be seen. Another advantage of having the mode patterns visually is that any shifting in the modes could be paired with the nonlinearities found in the data being retrieved.

2.1.4. Laser Diode Optical Test Fixture and Camera Setup

The optical box setup includes two die cast aluminum boxes of differing sizes that contain the laser diode and mounting devices that hold the laser diode. The camera setup includes three degrees of translation, a diode web-camera, and different microscope

objectives. The smaller box is 12cm long, 6.5cm wide and 3.5cm deep. The larger box is 19.5cm long, 11.5cm wide and 5.5cm deep. A 2.5cm diameter hole was cut into the shorter side wall of both boxes at one end to allow for the output of light from the laser diode for near and far field imaging. The larger box has four leg posts attached to an optical bench. Two rails were cut into the bottom of the larger box for the small box to be set into with the ability to slide the smaller box inside the larger box shown in Figure 16. The rails were cut with a dremel tool, and the attachment used was an abrasive wheel. The smaller box has four legs on the bottom side of the box which fit into the rails; this provides more range of focus for different magnifications. The rails also provide more movement in the y-direction for the measurements shown in Figure 16.

Inside the smaller box is a proto board with connection pins sticking upwards. The proto board is screwed into four posts that are attached to the smaller box. A holder for the laser diode slides onto the connector pins and holds the laser diode as seen in Figure 18 and Figure 19. Two of the connector pins were wired with coaxial lines for input and output of the laser diode. These two wires lead to BNC connectors on the derivative box. An arm, which is screwed into the bottom of the small box, holds the laser diode holder at a given angle for alignment purposes.

Three stages, which serve as a XYZ translation device, hold the camera and microscope objective. The X and Y directions are shown in Figure 16 and the Z direction is coming out of the page. Mounted on the front of the Z direction stage is the camera and objective lens holder. Epoxy was applied to a plastic mount for the camera and placed directly on a piece of metal with a threaded hole for the objective lens. The camera screws into the plastic piece on one side and the objective lens is screwed into the

other. This allows an image to be enlarged on the camera chip. The camera is hooked to a computer via USB cable and is controlled by LabView.

The purpose of this setup is to obtain electrical derivative measurements while observing the optical mode patterns and any irregularities that may be present. Using the microscope objective to image the optical pattern on the chip allows for a closer look at the near field. High power microscope objectives require a close working distance. Devices that are packaged with a protective cover (can) limit the magnification to about 20 X due to the space between the device and the protective window. We have operated the system with objectives up to 100X on devices with the chip exposed by removing the can. Below is the image of a proton VCSEL at 20X and 40X. A flash light was used to illuminate the diode, the one on the left is a hermetically packaged diode with a can, and the one on the right is a diode mounted on a header without a can. The glare in the right side of both pictures is the light reflected off of the wire bond to the chip. The 60X objective allowed for better viewing of the optical mode patterns. The magnifications lower than 60X did not display the near field images well enough to observe any optical mode changes.

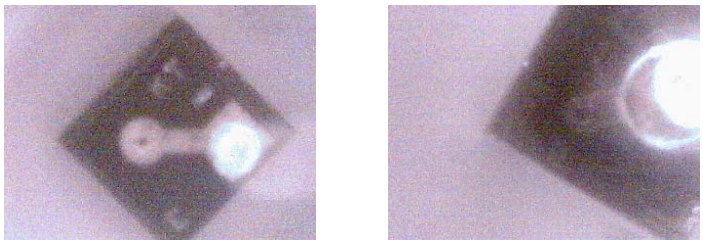

Figure 14 Proton bombarded VCSEL seen under 20x and 40x microscope objective lenses, the left VCSEL is packaged with a can on top of the chip, the right VCSEL does not have a can on top of the chip.

The 100X objectives have proved to be troublesome when trying to take images. The small working distance of the 100X objective is only a few micrometers. When

coming into focus the objective is very close to the wire bond and if the operator moves the objective too close then the objective crushes the wire bonded to the devices.

Another approach used to capture the near field images was to move the optical test fixture with the diode a set distance away from the camera. Two lenses with differing focal lengths are placed between the diode and the camera. The two lenses project the image of the VCSEL a distance corresponding to the focal lengths used. This approach allows for a large amount of magnification to be used. For reasons of limited space and availability of the optimum lenses this approach could only be tested for low magnification.

2.1.5. Problems Encountered

The camera setup has a problem that is easily solved with the proper amount of optical attenuation. When imaging the optical mode onto the camera a large amount of filtering is needed so that the camera is not saturated with light. If the camera becomes saturated, first the image bleaches white and with more saturation a dark spot appears at the most intense portion of the optical image. A filter of optical density (OD) 6 reduces the optical intensity by six orders of magnitude. Unfortunately six orders of magnitude have been determined too much filtering for this experiment because of the low currents used to test the diodes. The filter that is used in the test fixture was cut from laser goggles that had the proper amount of OD for wavelengths around 850 nm.

There are also electrical problems that occur occasionally. Any issues that occur with the derivative machine and test fixtures have many options to help resolve the

problem. Once the program is running, one option available to the user is to run the derivative machine in manual mode to test the accuracy of the interface cards present. The lock-in amplifier also has two electrical test points that allows the feedback from the device under test to be seen on an oscilloscope for viewing and subsequent troubleshooting for noise or other problems. If all else fails to solve the problem a full proof approach for troubleshooting is to systematically test every input and output point for irregular signals or missing signals.

2.1.6. Far Field Images

The optical camera test fixture can also be used to obtain the far field images. First the laser diode is setup in much the same way as when obtaining the near field image but the microscope objective is removed. A beam stop is placed a distance from the diode to display the far field image. After the beam travels an appropriate distance and expands the image, another camera is used in capturing the image. The camera used for far field imaging is a Logitech web camera that has the infrared (IR) filter removed and the case reassembled. No filtering is required because the light output is not directly imaged on the camera and does not saturate the camera.

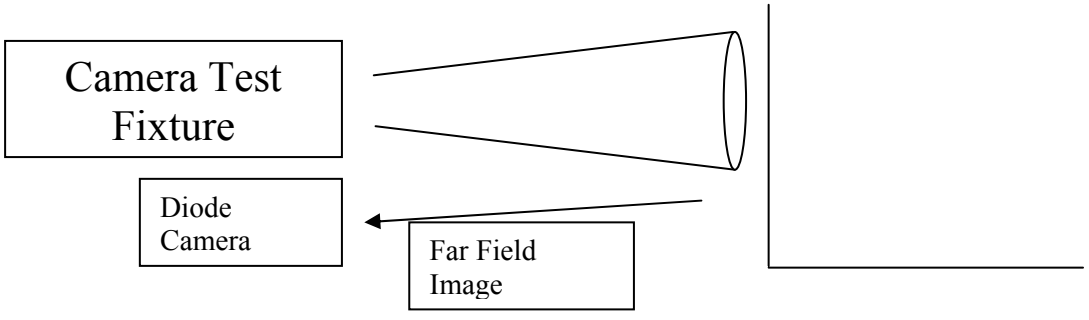

Figure 15 Block diagram of the far field image setup.

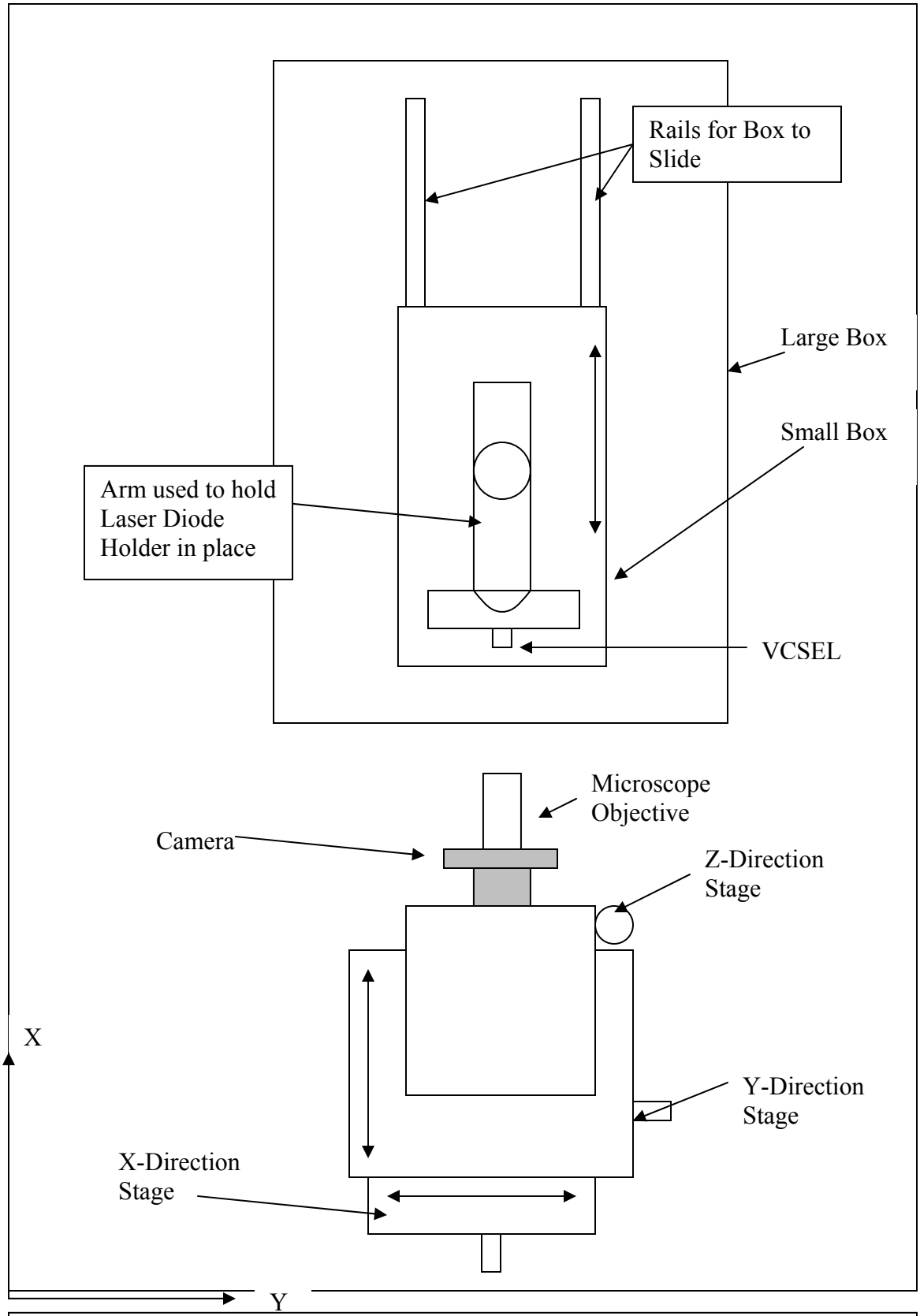

Figure 16 Block Diagram of the Camera Voltage Test Fixture.

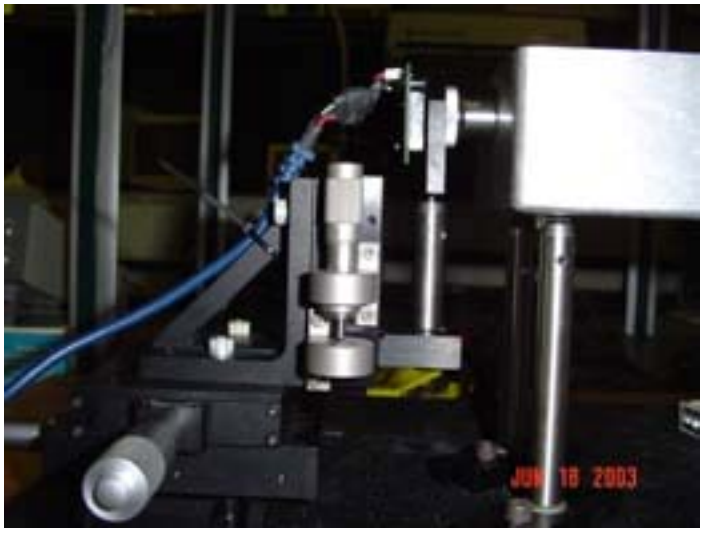

Figure 17 Three translation stages used to hold camera and objective lens for optical camera box.

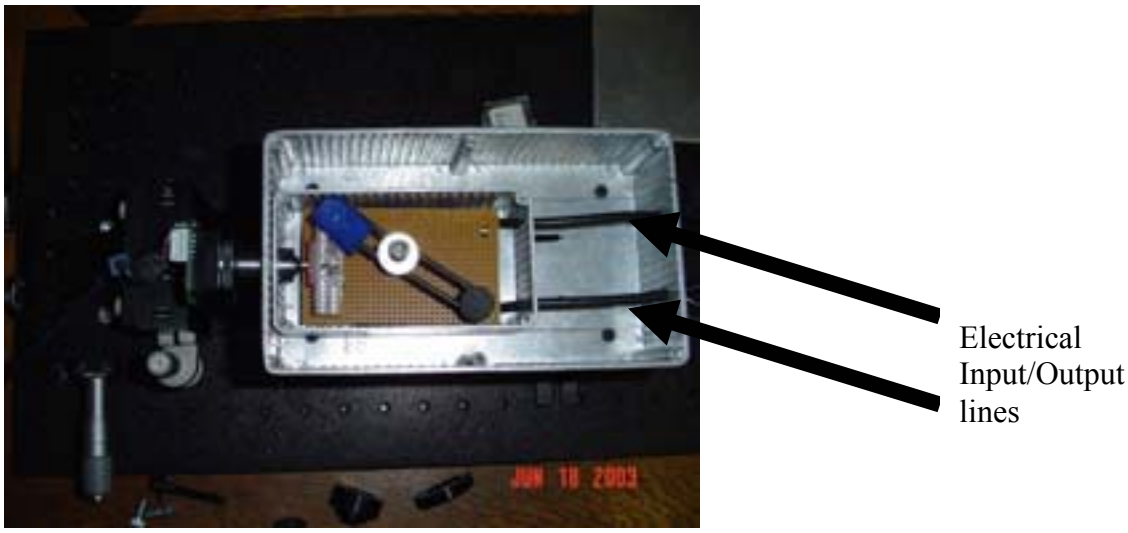

Figure 18 Full view of the Optical camera box.

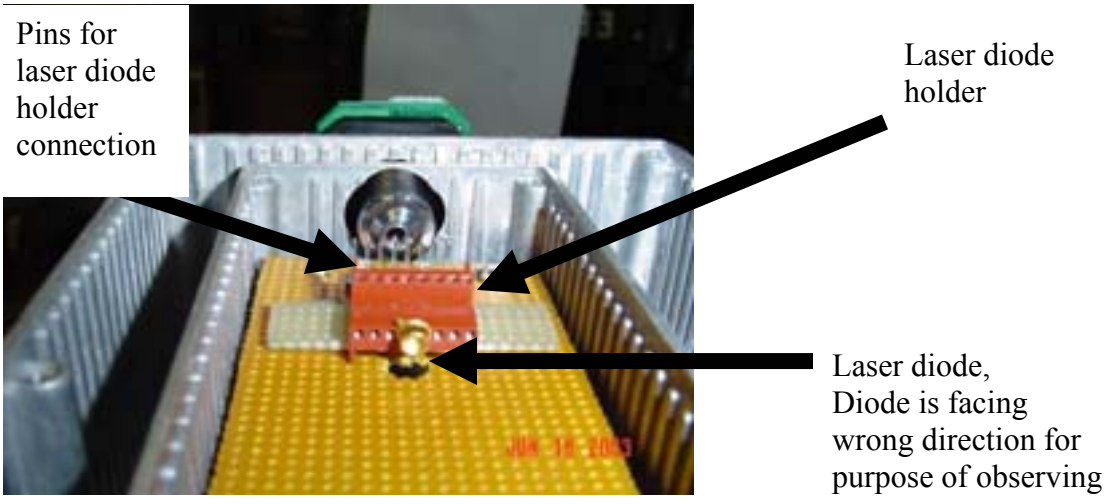

Figure 19 Optical box, connector pins and laser diode holder.

2.2. Programming Issues

The derivative machine was originally interfaced to a HP 300 model computer. This computer used the HP Basic language and an IEEE 488 bus to interact with the derivative machine. Since computers have become much faster and easier to use there was a need to switch from the older model HP computer to a new Dell 4500 desktop series. The computer programming language used on the PC is called Trans Era HT Basic, which is an upgrade of the HP Basic used in the HP 300 computer. The program needed few adjustments before being moved to the PC, for example the HP computer needed dynamic memory setup to be programmed, but the PC did not need this type of setup so a few lines of code had to be adjusted. Other minor adjustments were also made to make the program user friendly.

Once the program is running, a user is prompted to answer a number of questions. The first few questions are used to setup the derivative machine and set all interface cards used for input and output to zero. The next set of questions deals with the test devices and what type of measurement is to be taken. Limiting input values are also set at this point so the device is not over driven. Once all the questions are answered, the program runs the selected inputs through the test device while recording the responses from the device under test. The order of the measurements is as follows. First the program takes an I-V and L-V measurements at the same time, not only taking the data but determines when range changes and various limits should be set during subsequent measurements. Next the program runs through the first and second derivative of current measurements. Last measurement taken is the light derivative measurement. When taking the second

derivative, the voltage measurements are integrated over one or ten power line cycles (PLCs). Graphs and data are displayed on the computer screen to keep track of the data as it is acquired. Once the program has run its course, a few options become available to the user. Initial plots of the data just taken can be printed for evaluation of any visible undesirable data. Another option is for the data to be stored in a given file folder. The other options pertain to repeating the measurement or starting a different measurement.

After the data is acquired and stored in text files in a folder a graphing program, kaleidagraph, is used to plot the data. A short automated program was written with kaleidagraph to plot the data in a given format. The data can be plotted in pairs for comparison, for example the first and second derivative can be plotted on top of one another in different colors. Overlaying the plots help identify many of the irregularities found in the derivatives. Plotting the data in pairs is also helpful with respect to correlating the optical and electrical derivatives.

As mentioned earlier the program Labview is used to control the camera when taking the images of the optical modes while running the HT Basic program. In order to take a picture of the optical mode at every voltage step both the HT Basic and Labview programs had to be interfaced in some manner. While there is not to my knowledge a direct interface for these two programs a round about way of interaction is used. A loop was written into Labview to read a file that HT Basic accesses and writes a one or zero corresponding to different commands for the camera. HT Basic also writes information to another file corresponding to what measurement is being taken at that given point. This information is used for the name of the file to keep track of the image and which voltage measurement goes with the image.

2.3. Hardware Requirements

The derivative machine was built at the point where IEEE 488.1 was the standard for that type of bus communication, so in order to use the GPIB interface in the PC a PCI GPIB card was purchased and installed from National Instruments (NIGPIB). Overall the NIGPIB card is a great card but could not correctly interface with the derivative machine because a new IEEE 488.2 standard is being produced and the NIGPIB cards are not backwards compatible. Another PCI GPIB card was purchased from Agilent which has backwards compatibility for use in older systems.

As mentioned earlier the derivative machine includes an adc which can also be used as a digital multimeter (DMM). The adc is accurate up to five digits and works well for the derivatives, however the adc can not compare to an industrial DMM. A Keithley 2000 DMM is used for the derivative measurements. The Keithley DMM can be setup to integrate over the necessary amount of PLCs. Since the Keithley has an internal processor the speed and accuracy surpasses the custom built adc interface card.

3. Chapter 3 – VCSEL Measurements and Observations

3.1. Measurements of Proton Defined VCSELs

The Proton VCSEL structure consists of two DBR mirrors (one on top and one on bottom, a region of proton damage, active region. The proton bombarded layer provides good current confinement but little or no optical confinement. The active region consists of multiple quantum wells. An example of the proton structure can be seen in Figure 4. The two measurement fixtures used on the devices under test, mentioned in chapters 2.1.3 and 2.1.4 above, to obtain different observational and numerical data. With the plotting program Kaleidagraph different graphs can be obtained, using the electrical and optical numeric data. The voltage test fixture provides I-V, dI/dV, d^2I/dV^2, L-V, dL/dV measurements and the camera test fixture provides I-V, dI/dV, d^2I/dV^2. The camera fixture provides near-field images but does not take optical power measurements. Both test fixtures take the same electrical data and produce the same plotted results for a given device. Chapter 3.1 will discuss how recorded near-field observations are used in conjunction with the plotted electrical signals from the proton VCSELs to show correlations between derivative peaks, lows, and "warts".

3.1.2. Simple Electrical and Optical Relationships (Proton)

To better understand the inner workings of proton defined VCSELs, it is desirable to understand the correlation of the electrical and optical signals in the device. The

literature has a vast body of work relating the light output to the current input[13]. A simple relationship is observed between the current vs. voltage and the light output versus voltage and/or current, as shown in Figure 20. This plot shows a flat region before laser action and at threshold a rising curve indicating a rapid rise in either current or light output.

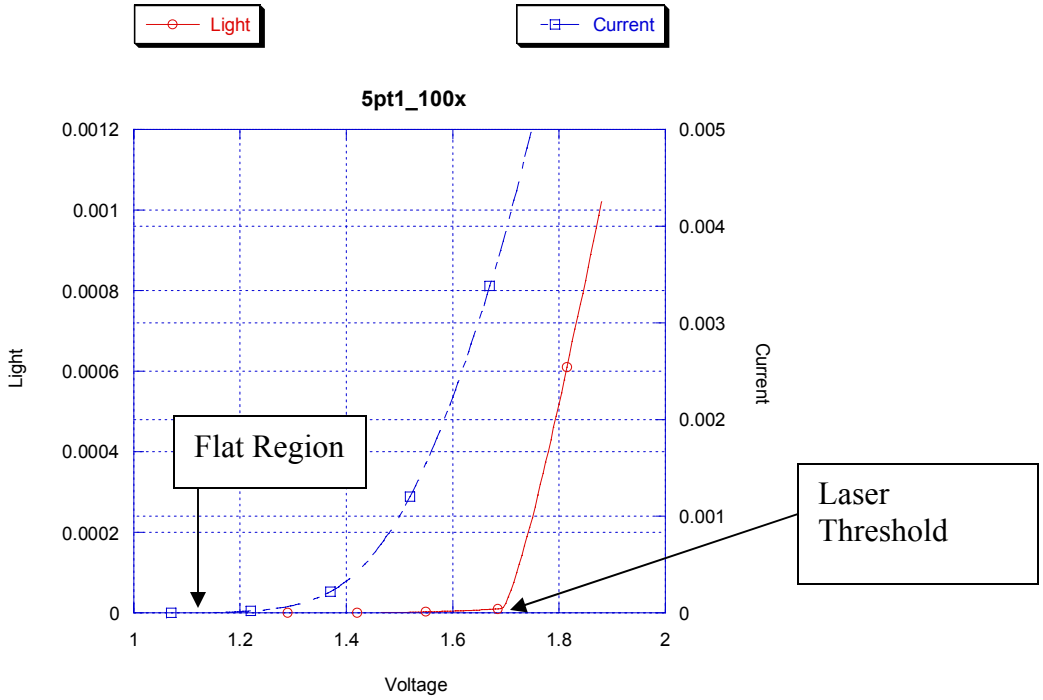

Figure 20 Current versus voltage and light versus voltage measurements plotted on the same graph to show similarities. The similarities start with the flat region before laser threshold, after laser threshold both curves have rapidly rising slopes.

The current rises in the blue curve (I-V) due to a rapid increase in injected carriers, and then around 1690 mV (~3.75 mA), laser threshold, the curve becomes nearly linear again.

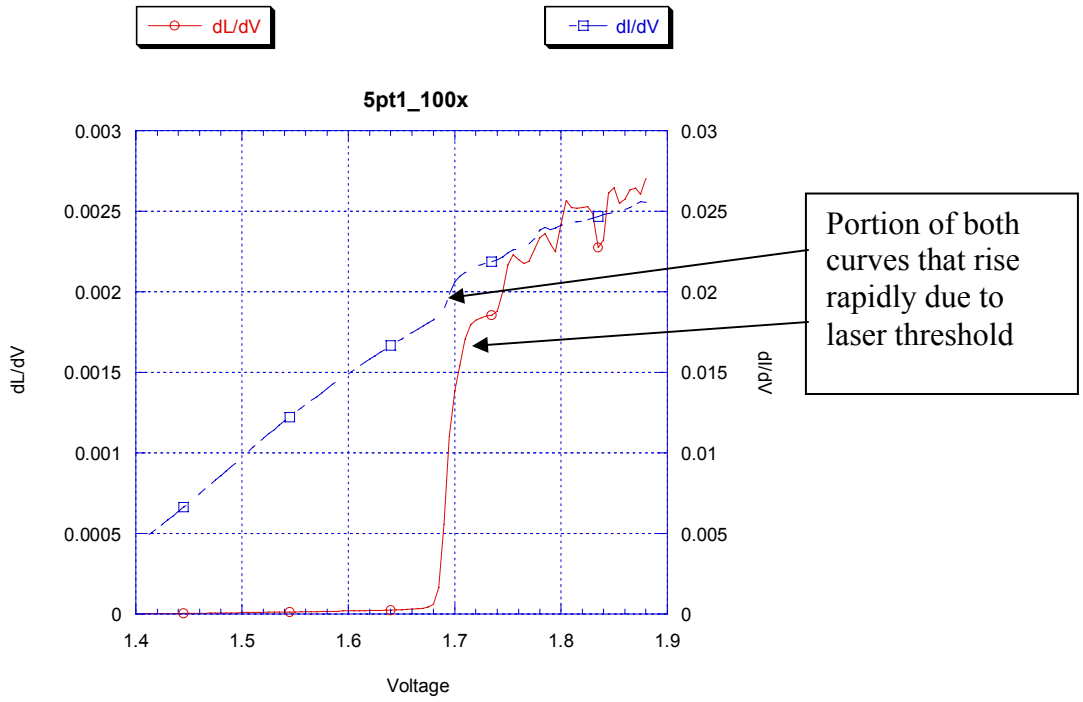

Figure 21 First derivative of the light and current versus voltage. The first derivative curves show a sharp rise at laser threshold and role over at approximately the same drive voltage.

Light derivatives show some of the same characteristics as the current derivatives. The dL/dV curve is a measure of how efficient the light output is to the amount of drive voltage. The extreme rise in the red curve (dL/dV) suggests a large increase of light for a small increase of input voltage. This corresponds to laser threshold, with a vertical rise in the blue conductance curve (dI/dV). The dI/dV curve is the conductance of a device, which also shows a large rise in current for a very small amount of voltage as seen in Figure 21. After threshold both curves also start to roll over to another slope at 1720mV (~ 5.02mA). The mechanism that causes this roll over effect has not yet been explicitly identified. First derivative measurements reveal different processes happening within the device under test and the second derivative is very helpful in identifying small changes in the first derivative.

Second derivative measurements highlight nonlinearities that are difficult to see in the first derivative. A first and second derivative plot will directly correspond due to the mathematical relationship; any slope change in the first derivative will have a minimum or maximum in the second derivative as shown in Figure 22.

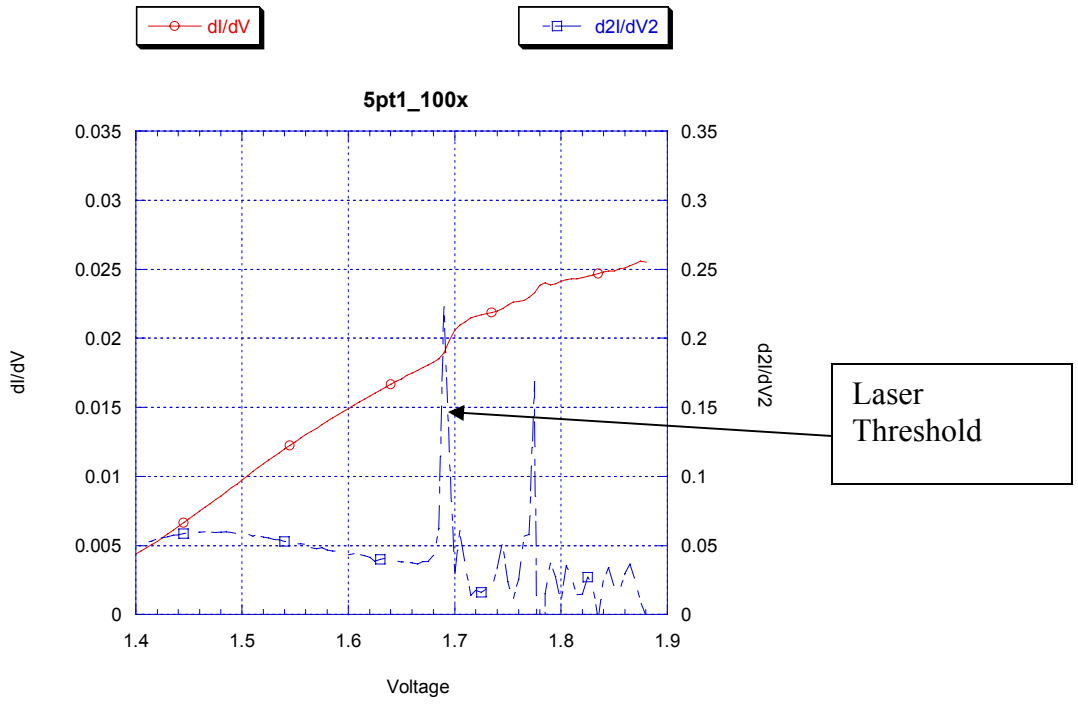

Figure 22 First and Second derivative plots. The first bulge in the second derivative is the spontaneous emission of the device, this part of the curve directly relates to the change slope in the first derivative. The large peak in the second derivative shows laser threshold, this peak highlights the slope change in the first derivative.

The second derivative has a broad maximum around 1500 mV (~1.06 mA), a large spike at 1690 mV (~ 3.75mA), and a small amount of structure from 1720 mV to 1880mV (~ 4.365mA to 8.25mA). The first broad maximum in the second derivative corresponds to spontaneous emission from the device. The large peak in the second derivative reveals laser threshold, which corresponds to the rapid rise in the conductance at threshold. At yet high voltages (currents) the second derivative has additional peaks which correspond to more slope changes in the first derivative. Since the first derivative

of both the light and current with respect to voltage had a relation, the second derivative should also highlight any nonlinearity in the light derivative.

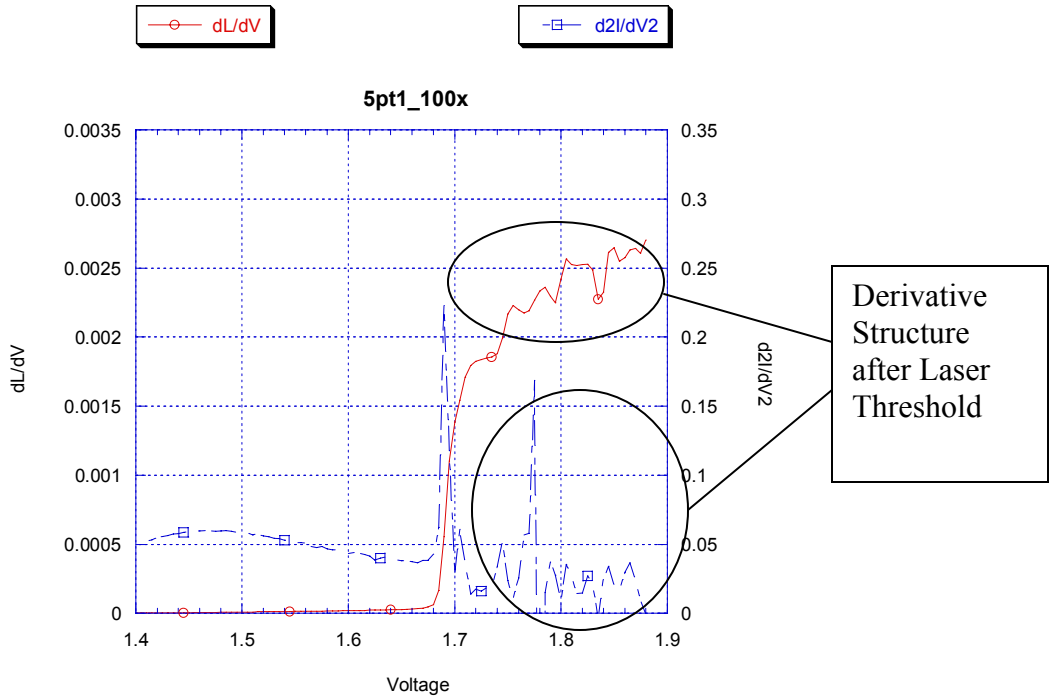

Figure 23 First derivative of Light (dL/dV) and Second derivative of the current (d2I/dV2). The first peak in the second derivative corresponds to the sharp rise in the first derivative of light. There is additional structure in the plots after threshold.

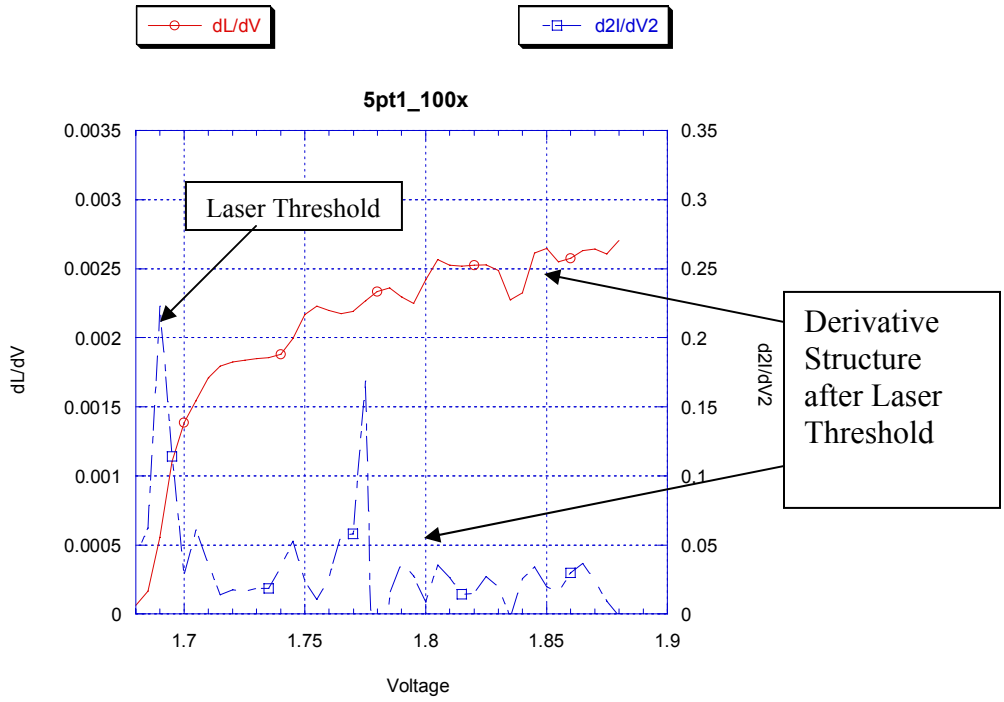

Figure 24 First derivative of Light and Second derivative of Current zoomed in to view the structure of both plots.

The first derivative of the light (dL/dV) shows a small amount of structure after laser threshold. This structure is also demonstrated in the second derivative of the current in Figure 23. An expanded view of both plots is shown in Figure 24.

We now wish to determine whether there is correlation between stable electrical characteristics and stable optical modes. This was done using the camera test fixture. Laser threshold is the easiest mechanism to view because of the large increase in optical intensity for a small increase in forward bias.

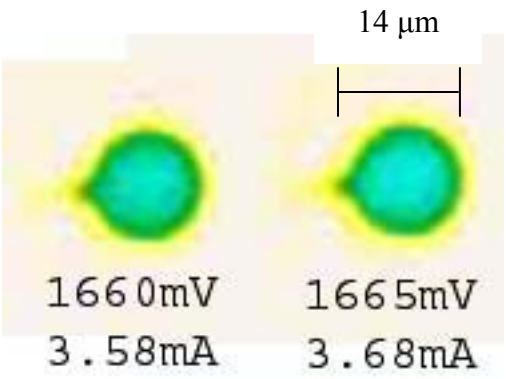

Figure 25 (Left) Proton number five test run five, 1660mV (~ 3.58mA) just before laser threshold. (Right) Proton number five test run five, 1665mV (~ 3.68mA) laser threshold. An increase in the light intensity can be seen from left to right. The image has been false colored to better view the change light intensity.

The proton VCSELs show a large increase in optical intensity at laser threshold. The intensity count just before laser threshold at 1660mV (~ 3.58mA) is approximately 2528, then after threshold the count moves up to approximately 3015. The original image was false colored to better view the change in intensity.

3.1.3. Optical Mode Stability (Proton)

Optical mode stability is important in many laser applications. Optical modes can shift to lase in different positions in the optical cavity as the spatial dependence of the gain shifts[9]. Figure 26 depicts laser filaments above laser threshold.

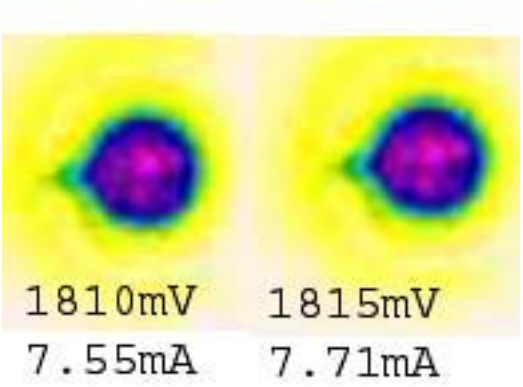

Figure 26 Modal pattern of Proton number five test number five. These images show the optical modes at 1810mV (~ 7.55mA) and 1815mV (~ 7.71mA), above laser threshold 1665mV (~ 3.68mA).

In a proton defined VCSEL cavity the proton bombarded area provides current confinement. The damaged area also provides a very small amount of optical confinement. In this case laser filaments start to lase at different drive voltages. The regions of higher activity are filaments lasing in the gain media. The first derivative of light shows structure after threshold, however the light output still increases proportionally with the current. This fact is also shown in the array of near field photos in Figure 27.

Figure 27 Array of output intensity images for Proton VCSEL number five test number five.

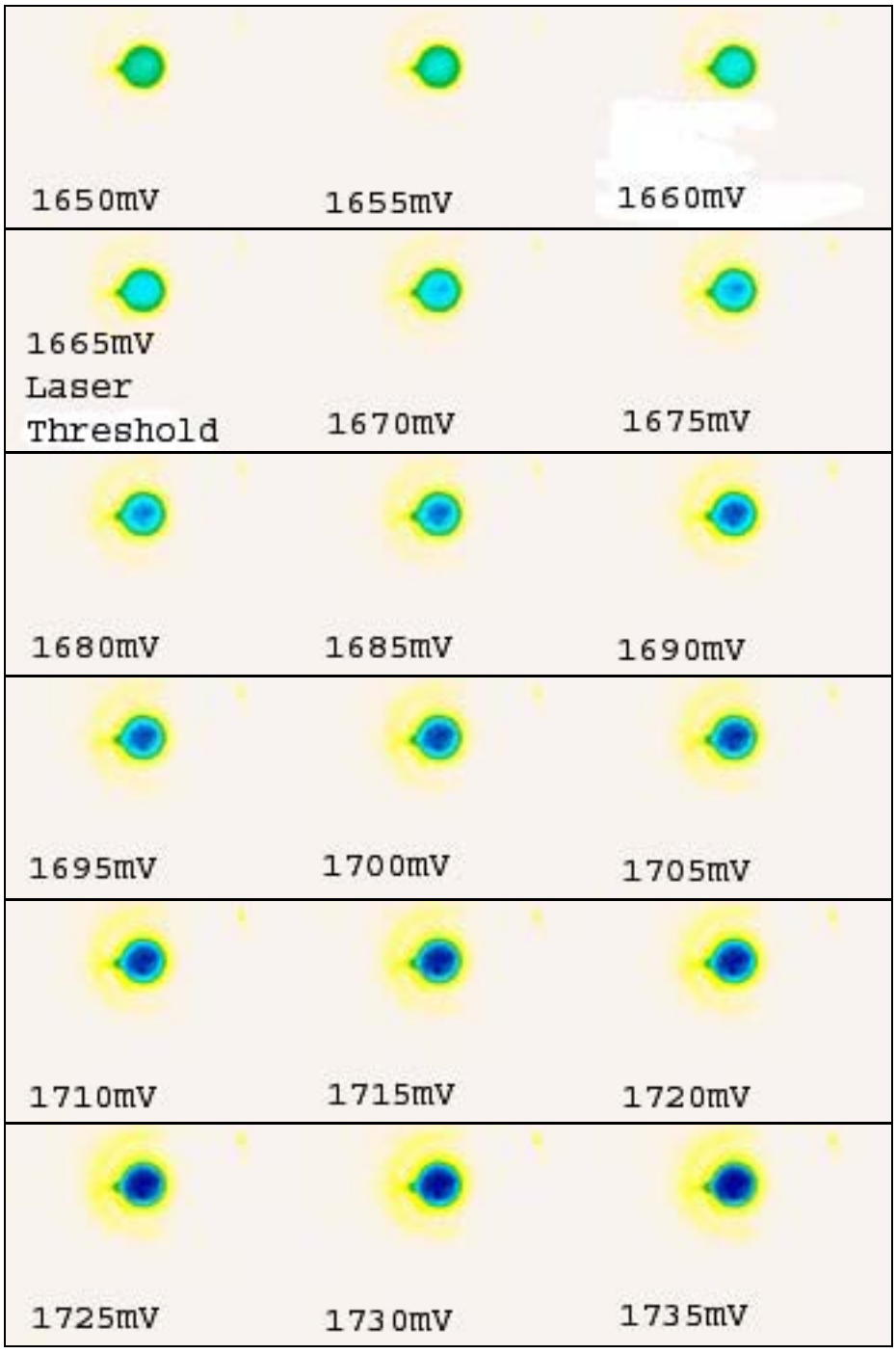

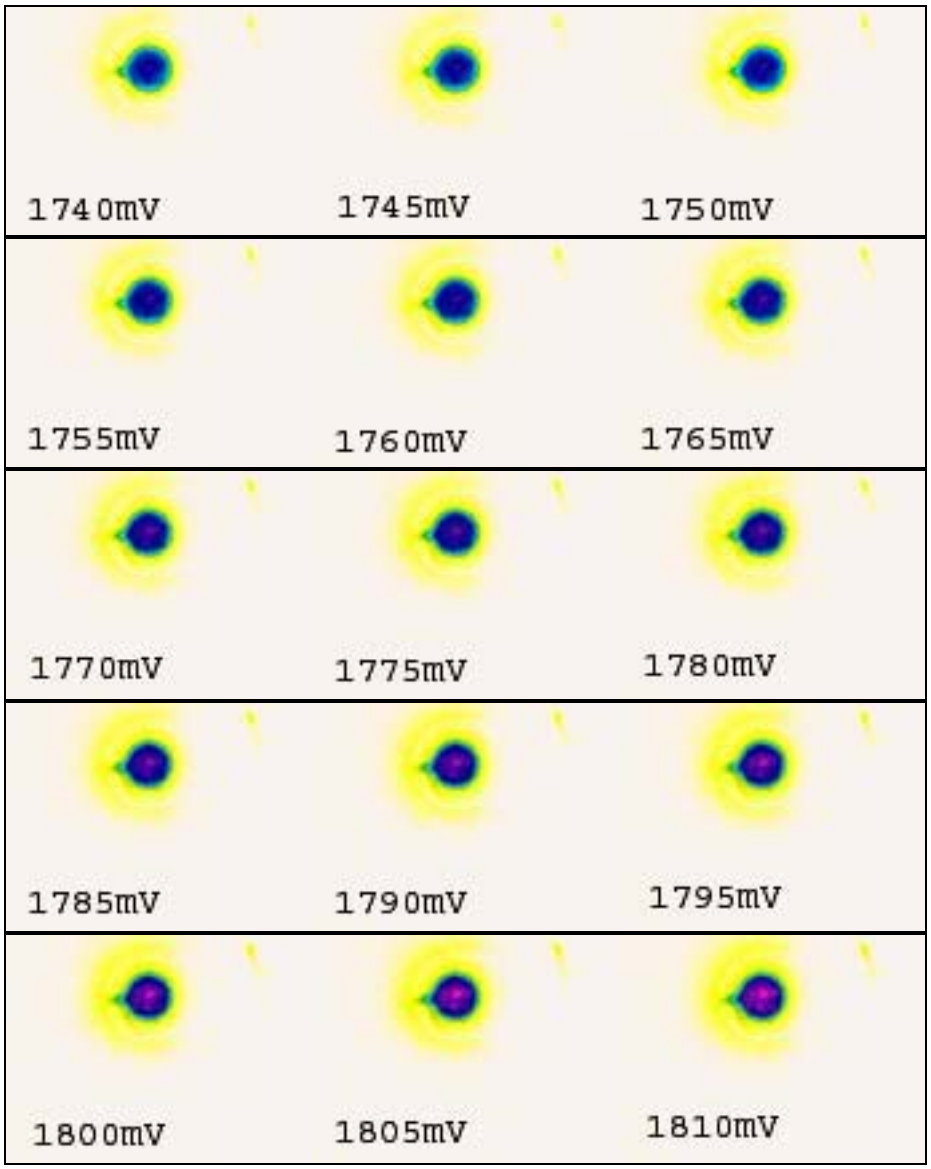

3.2. Measurements of Oxide Defined VCSELs

The Oxide VCSEL structure consists of two DBR mirrors (one on top and one on bottom, a layer of oxide, active region. The oxide layer provides good current and optical confinement. The active region consists of multiple quantum wells. An example of the oxide structure can be seen in Figure 4. The two measurement fixtures used on the

devices under test, mentioned in chapters 2.1.3 and 2.1.4, to obtain different observational and numerical data. With the plotting program Kaleidagraph different graphs can be obtained, using the electrical and optical numeric data. The voltage test fixture provides I-V, dI/dV, d^2I/dV^2, L-V, dL/dV measurements and the camera test fixture provides I-V, dI/dV, d^2I/dV^2. The camera fixture provides near-field images but does not take optical power measurements. Both test fixtures take the same electrical data and produce the same plotted results for a given device. Chapter 3.2 will discuss how recorded near-field observations are used in conjunction with the plotted electrical signals from the oxide VCSELs to show correlations between derivative peaks, lows, and "warts".

3.2.2 Simple Electrical and Optical Relationships (Oxide)

To better understand the inner workings of oxide defined VCSELs, it is desirable to understand the correlation of the electrical and optical signals in the device. The literature has a vast body of work relating the light output to the current input[13]. A simple relationship is observed between the current vs. voltage and the light output versus voltage and/or current, as shown in Figure 28. This plot shows a flat region before laser action and at threshold a rising curve indicating a rapid rise in either current or light output.

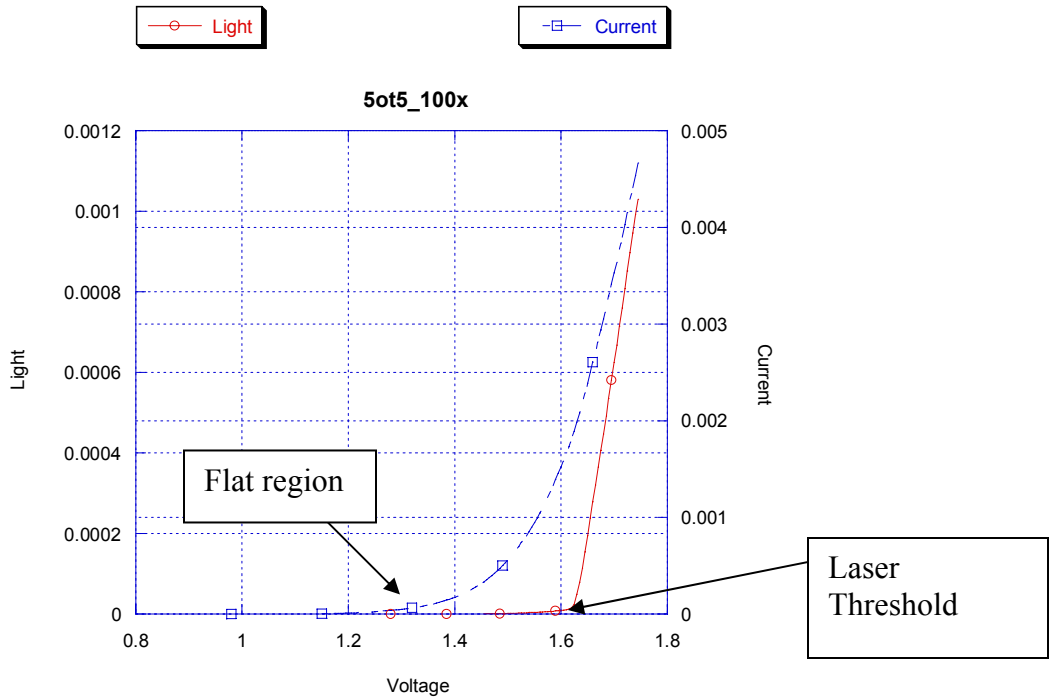

Figure 28 Current versus voltage and light versus voltage measurements plotted on the same graph to show similarities. The similarities start with the flat region before laser threshold, after laser threshold both curves have rapidly rising slopes.

The current rises in the blue curve (I-V) due to a rapid increase in injected carriers, and then around 1620 mV (~1.8 mA), laser threshold, the curve becomes nearly linear again.

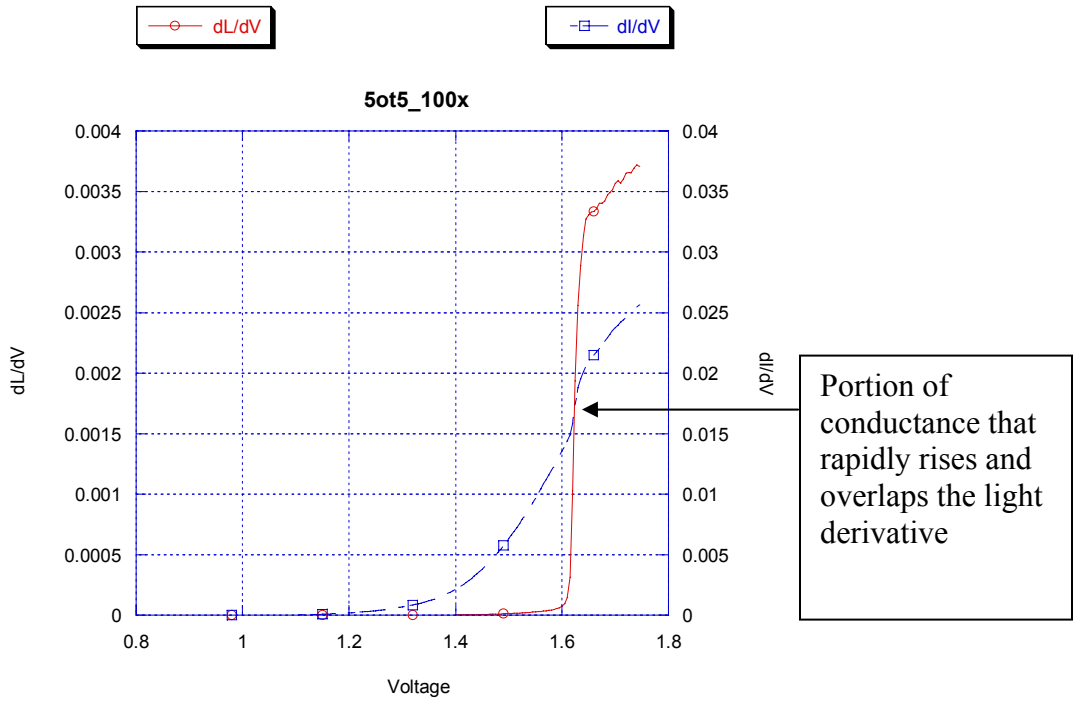

Figure 29 First derivative of the light and current versus voltage. The first derivative curves show a sharp rise at laser threshold and role over at approximately the same drive voltage.

Light derivatives show some of the same characteristics as the current derivatives. The dL/dV curve is a measure of how efficient the light output is to the amount of drive voltage. The extreme rise in the red curve (dL/dV) suggests a large increase of light for a small increase of input voltage. This corresponds to laser threshold, with a vertical rise in the blue conductance curve (dI/dV). The dI/dV curve is the conductance of a device, which also shows a large rise in current for a very small amount of voltage as seen in Figure 29. After threshold both curves also start to roll over to another slope at 1650mV (~ 2.39mA). The mechanism that causes this roll over effect has not yet been explicitly identified. First derivative measurements reveal different processes happening within the device under test and the second derivative is very helpful in identifying small changes in the first derivative.

Second derivative measurements highlight nonlinearities that are difficult to see in the first derivative. A first and second derivative plot will directly correspond due to the mathematical relationship; any slope change in the first derivative will have a minimum or maximum in the second derivative as shown in Figure 30.

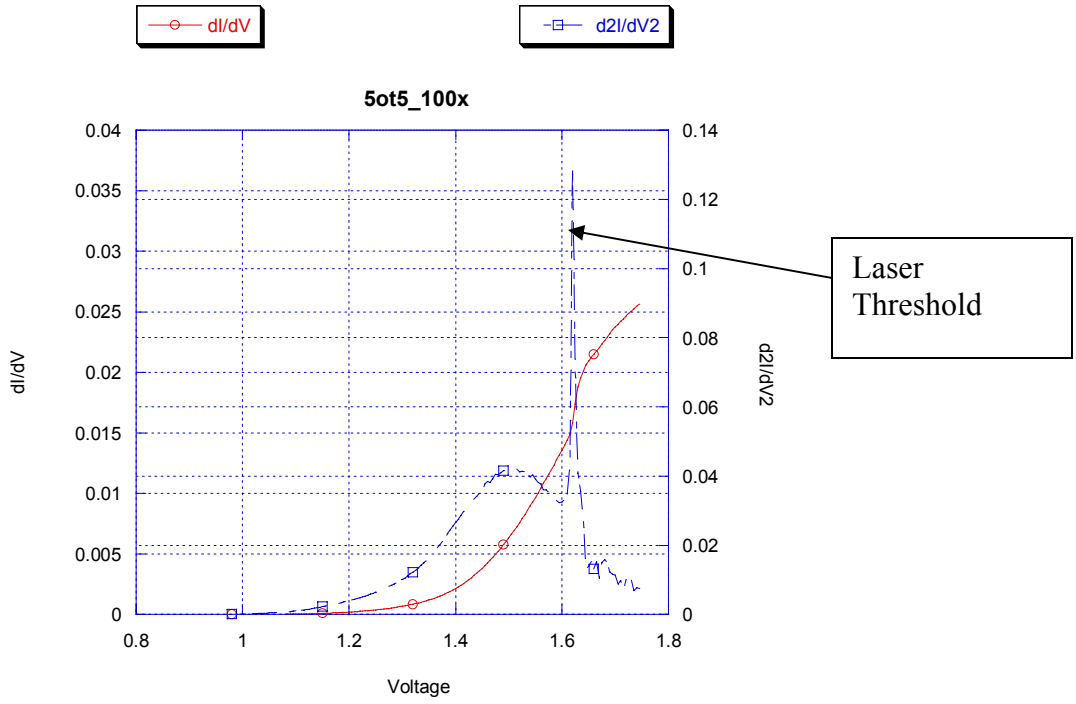

Figure 30 First and Second derivative of current versus voltage. The first maximum in the second derivative corresponds to spontaneous emission from the device. The large peak in the second derivative shows laser threshold, this peak highlights the slope change in the first derivative.

The second derivative has a broad maximum around 1500 mV (~.563 mA), a large spike at 1620 mV (~1.81 mA), and a small amount of structure from 1650 mV to 1745 mV (~ 2.39 mA to 4.67 mA). The first broad maximum in the second derivative corresponds to spontaneous emission from the device. The large peak in the second derivative reveals laser threshold, which corresponds to the rapid rise in the conductance at threshold. At yet higher voltages (currents) the second derivative has peaks which

correspond to more slope changes in the first derivative but these are much smaller than the amount observed at threshold. Since the first derivative of both the light and current with respect to voltage had a relation, the second derivative should also highlight any nonlinearity in the light derivative.

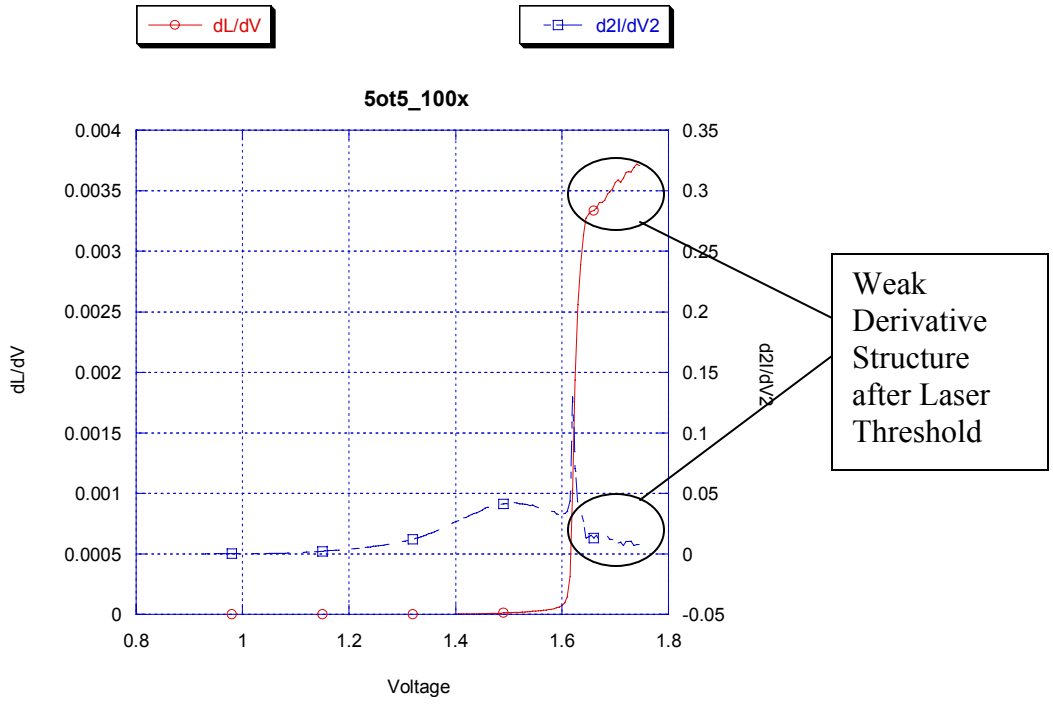

Figure 31 First derivative of Light (dL/dV) and Second derivative of the current (d^2I/dV^2). The peak in the second derivative corresponds to the sharp rise in the first derivative of light. There is a small amount of structure in the plots after threshold.

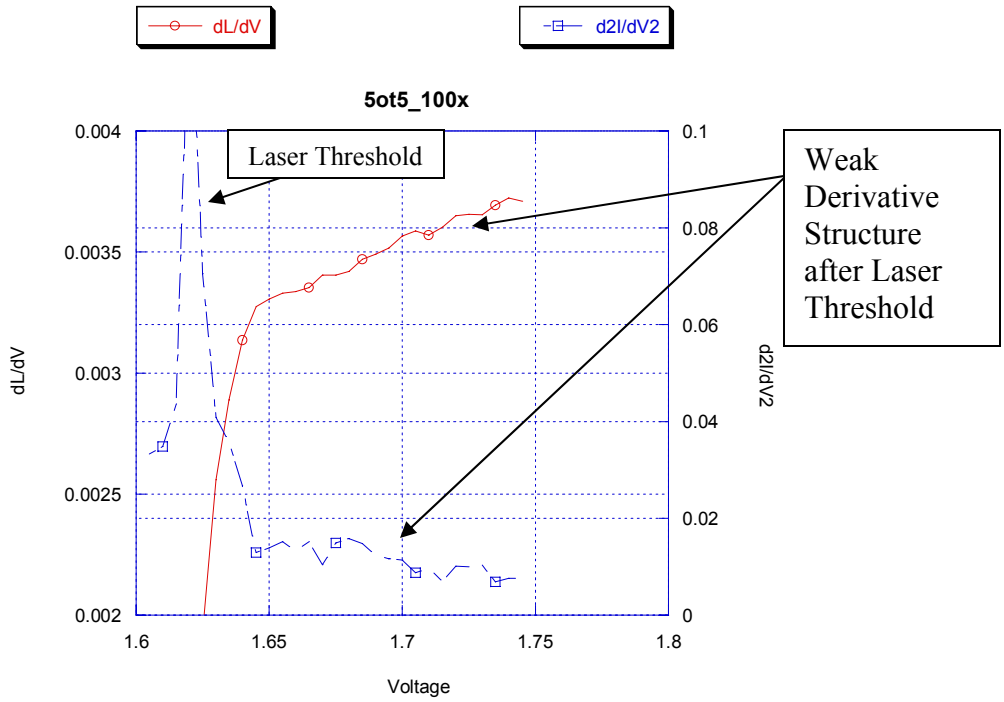

Figure 32 First derivative of Light and Second derivative of Current zoomed in to view the structure of both plots.

The first derivative of the light (dL/dV) shows a small amount of structure after laser threshold. This structure is also demonstrated in the second derivative of the current in Figure 31. An enlarged view of both plots is shown in Figure 32.

We now wish to determine whether there is correlation between stable electrical characteristics and stable optical modes. This was done using the camera test fixture. Laser threshold is the easiest mechanism to view because of the large increase in optical intensity for a small increase in forward bias. Near field mode patterns of oxide VCSELs have been obtained in previous literature where multiple modes were observed after the laser threshold[14].

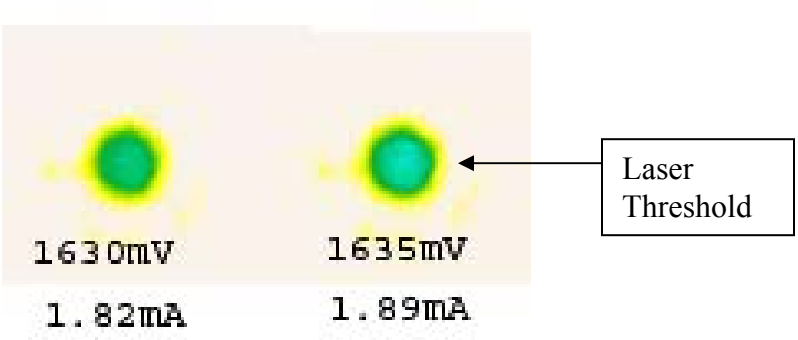

Figure 33 (Left) Oxide number six test run nine, 1630mV (~ 1.82mA) just before laser threshold. (Right) Oxide number six test run nine, 1635mV (~ 1.89mA) laser threshold. An increase in the light intensity can be seen from left to right. The image has been false colored to better view the change light intensity.

The Oxide VCSELs show a large increase in optical intensity at laser threshold. The intensity count just before laser threshold at 1630mV (~ 1.82mA) is approximately 3107, then after threshold the count moves up to approximately 3581. The original image was false colored to better view the change in intensity.

3.2.3 Optical Mode Stability (Oxide)

Optical mode stability is important in many laser applications. Optical modes can shift to lase in different positions in the optical cavity as the spatial dependence of the gain shifts[9]. Multiple laser modes have been observed in VCSELs with near field spectroscopy[14]. Figure 34 depicts laser modes above laser threshold. The "C" shaped modal pattern is most likely due to the p-side metal contact having an open portion corresponding to the open portion of the "C" shape. With reduced current flow to that portion of the active region light output can not be sustained in that region. The edge of the output aperture seems to be the only portion with enough current flow to start laser

action. The center of the output aperture is not lasing because of non-uniform current flow through the active region. The observed mode pattern is also influenced by the allowed optical modes as determined by the boundary conditions.

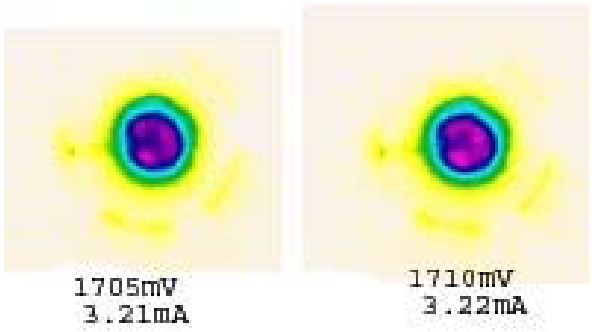

Figure 34 Modal pattern of Oxide number six test number nine. These images show the optical modes at 1705mV (~ 3.21mA) and 1710mV (~ 3.22mA), above laser threshold 1635mV (~ 1.89mA). The center of the cavity does not seem to have as much laser action as the perimeter of the output aperture.

In an oxide confined VCSEL the oxide provides current and optical confinement for the active region. Good optical confinement helps stabilize laser action after threshold. In this case the laser modes that start to lase at threshold are stable over a relatively large range of current. Figure 34 illustrates the fact that after threshold only a small amount of optical mode shifting activity can be seen. The first derivative of light illustrates that after threshold the light output still increases proportionally with the current. This fact is also shown in Figure 35.

Figure 35 Array of output intensity images for Oxide VCSEL number six test number nine.

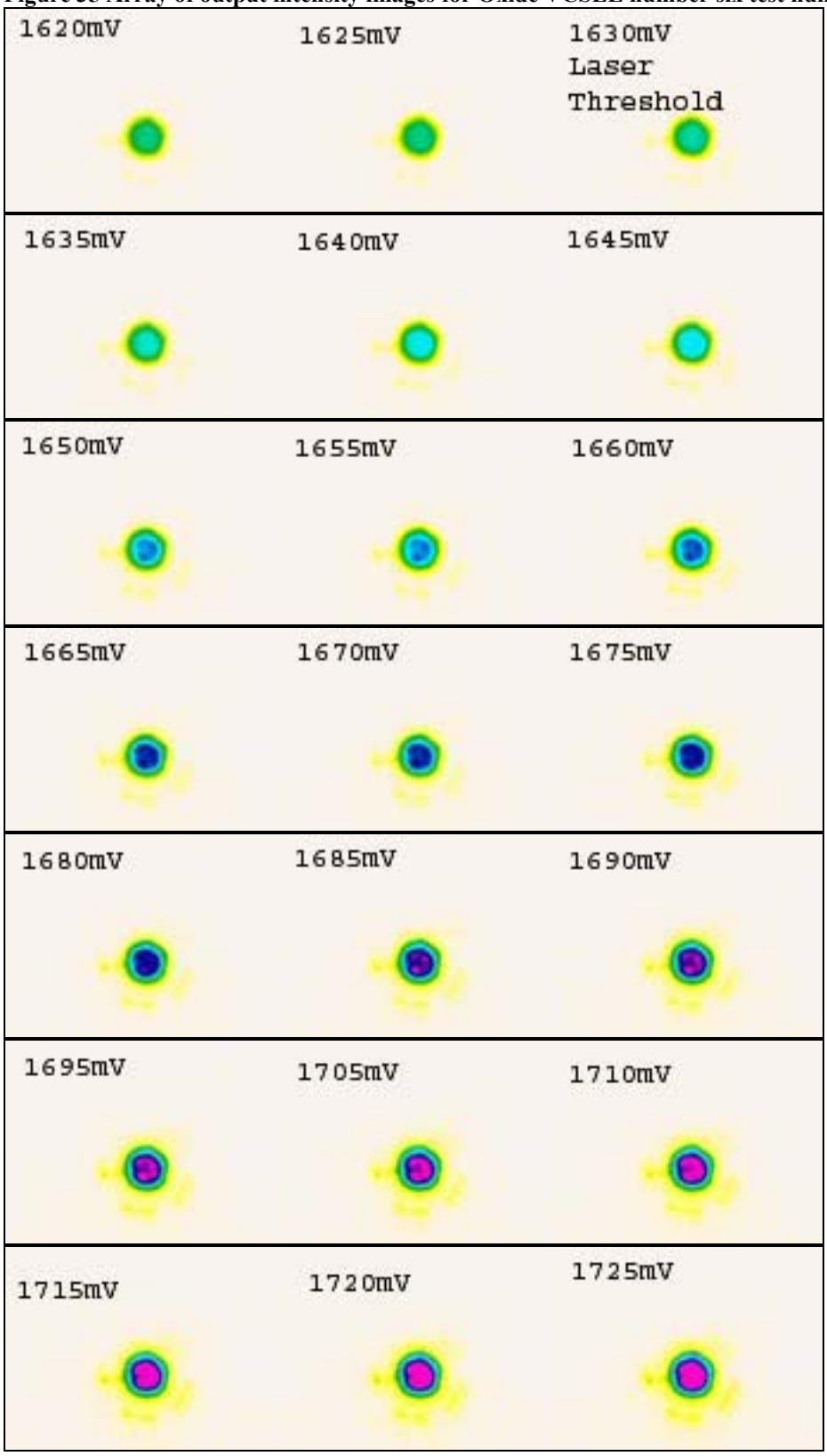

4. Chapter 4 – Analysis of Proton Data and Comparison of Results

4.1. Overview

Using the L-V and I-V curves simple relationships between light and electrical signals were shown in chapter 3.1.2. More complex relations can also be observed when looking at the light and current derivative curves of these VCSELs (dL/dV, dI/dV, d^2I/dV^2). To better understand the correlations made between the light and current derivatives near-field images are investigated. The light derivatives and the near-field images are shown to be directly related and with the simple relationships between the light and current derivatives, the electrical signals can also be related to the optical observations.

Three mechanisms have been identified as the cause of the derivative structure found after threshold in these devices. These mechanisms are discussed in the following chapters.

4.2. Near Field Optical and Derivative Measurements in Proton Defined VCSEL

Optical output patterns for a particular VCSEL are unique and reproducible for different test runs. The reproducibility of the output patterns reinforces the reproduced derivative structure for the VCSEL. If a different optical pattern were to occur during each test then we would expect the derivative structure to change from run to run also.

Given the reproducible results for both the derivative structure and optical mode patterns three distinct mechanisms can be observed. The first mechanism is laser action

or the start of a new filament in a particular portion of the active region. Laser threshold is the primary example of this mechanism. A new laser mode that starts shows a rapid rise in current and light for a small rise in voltage. The first derivative of light also displays a distinct rise in light output efficiency. In turn each additional laser mode or filament that starts to lase should display a sharp rise in dL/dV and dI/dV with a corresponding peak in the d^2I/dV^2 curve. This can be seen in Figure 36.

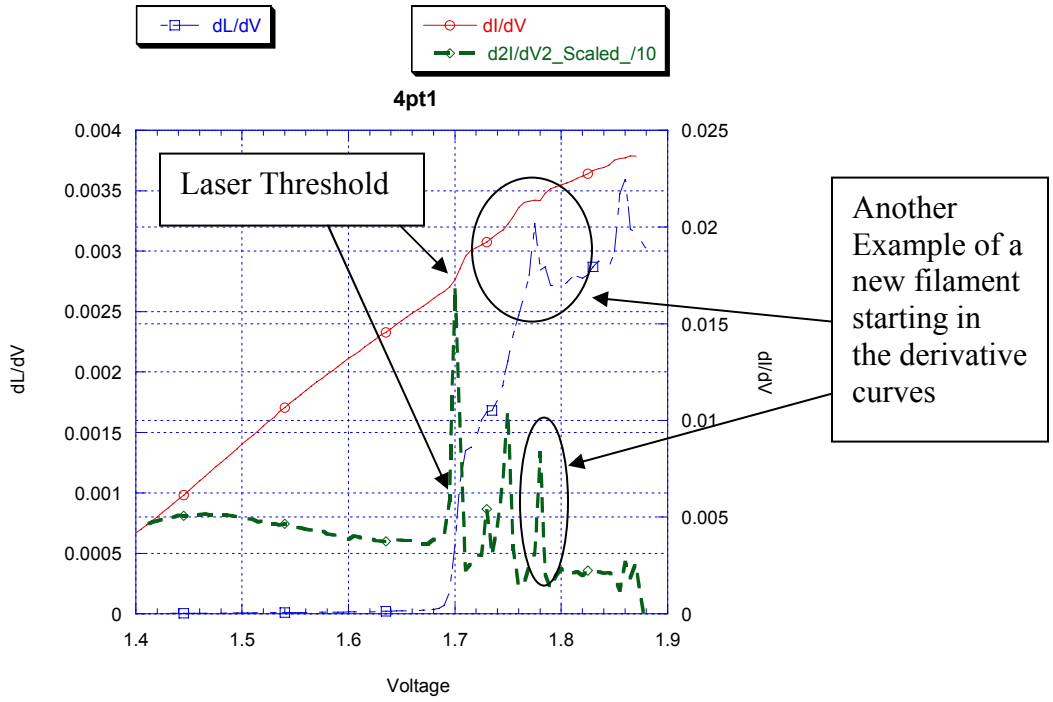

Figure 36 The first mechanism is seen at threshold where a new laser mode is formed. Note that at threshold there is a rapid rise in dI/dV, dL/dV, and a narrow peak in d^2I/dV^2.

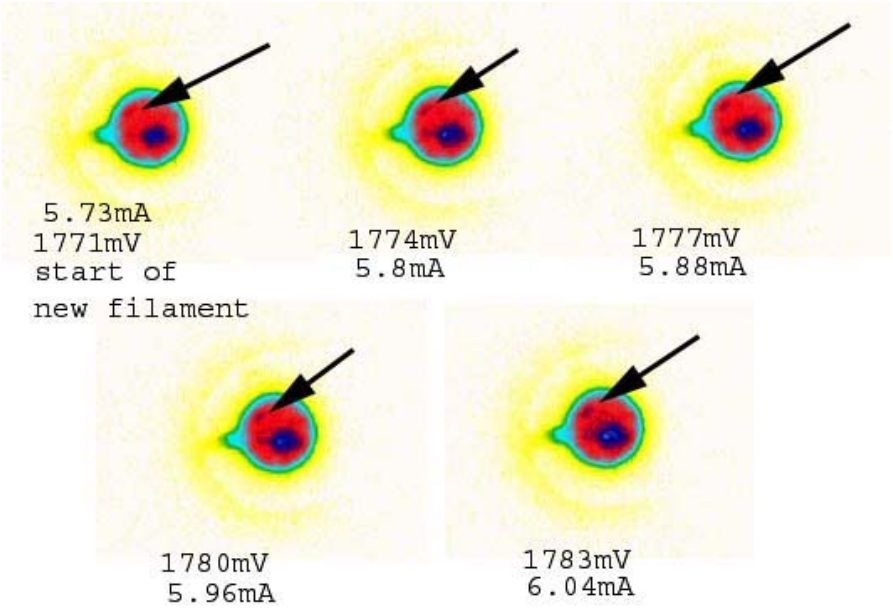

Figure 37 New mode starts at ~1770mV pointed out by the arrow. These modal patterns correspond with the derivative curves in Figure 36.

An example of a new laser filament starting above threshold is observed at ~1.770V in Figure 36. The corresponding modal patterns are shown in Figure 37 as a function of applied voltage. The location of the new filament is pointed out by the arrows in Figure 37. This filament starts to lase at ~1770mV. Prior work using narrow stripe geometry lasers has shown that the quasi Fermi levels lock (or saturate) after the onset of stimulated emission.[5] This mechanism is responsible for the rapid rise in the conductance, dI/dV, at threshold. It is best observed in homogeneous small geometry devices with minimal variation in the current distribution across the active region.[5]

Unfortunately VCSELs have a large emission aperture with a non uniform current distribution. Hence, to model the devices investigated, the active region is conceptually divided into an interconnected mesh of smaller individual laser diodes. These smaller

diodes can start to lase at different input voltages and have different geometries. An example of this model can be viewed in Figure 38.

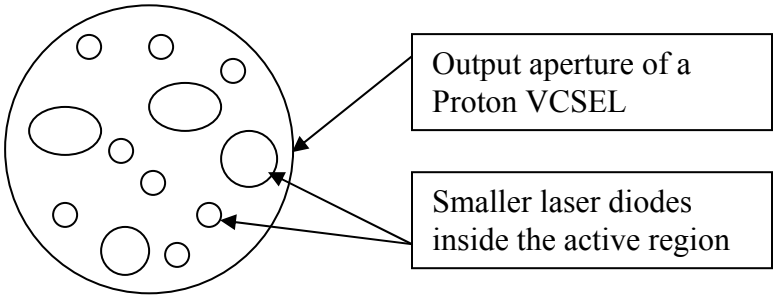

Figure 38 Representation of output aperture of a proton VCSEL with a number of smaller laser filaments inside the active region of the device. The random mode pattern may be due to low optical confinement allowing different regions to lase better than others.

At laser threshold a portion of the active region is found to start lasing which corresponds to a sharp rise in all three derivative curves. The quasi-fermi levels are expected to lock for that particular portion of the active region. At higher drive voltages above threshold other portions of the active region turn on and start laser action corresponding to the rapid rise in light and current derivative curves as seen in Figure 36 and Figure 37.

A second mechanism responsible for the derivative structure is the spatial shifting of a laser filament. One explanation for a spatial shift of a laser filament is that a new section of the active region provides a better (lower resistance) path to the current. This change in the preferred path of the current could be due to localized heating, current crowding, etc but the specific cause is not important at this point, only that the shift can happen. Under these circumstances one would expect the conductivity to increase but not as rapidly as the core of a new mode developing. One would also expect only minor variations in the light output since no additional new laser filaments evolve, only spatial shifting of the existing filaments. These trends appear in the derivative measurements in the voltage range from ~1800mV to 1850mV in Figure 39. Based on the derivative plot

in Figure 39 a new filament appears to be forming between 1830mV and 1850mV (sharp rise in d^2I/dV^2) but it never attains a strong narrow d^2I/dV^2 peak. Rather, as seen in Figure 40, the modes shift spatially about the active region while the optical derivative dL/dV remains almost constant as seen in Figure 39.

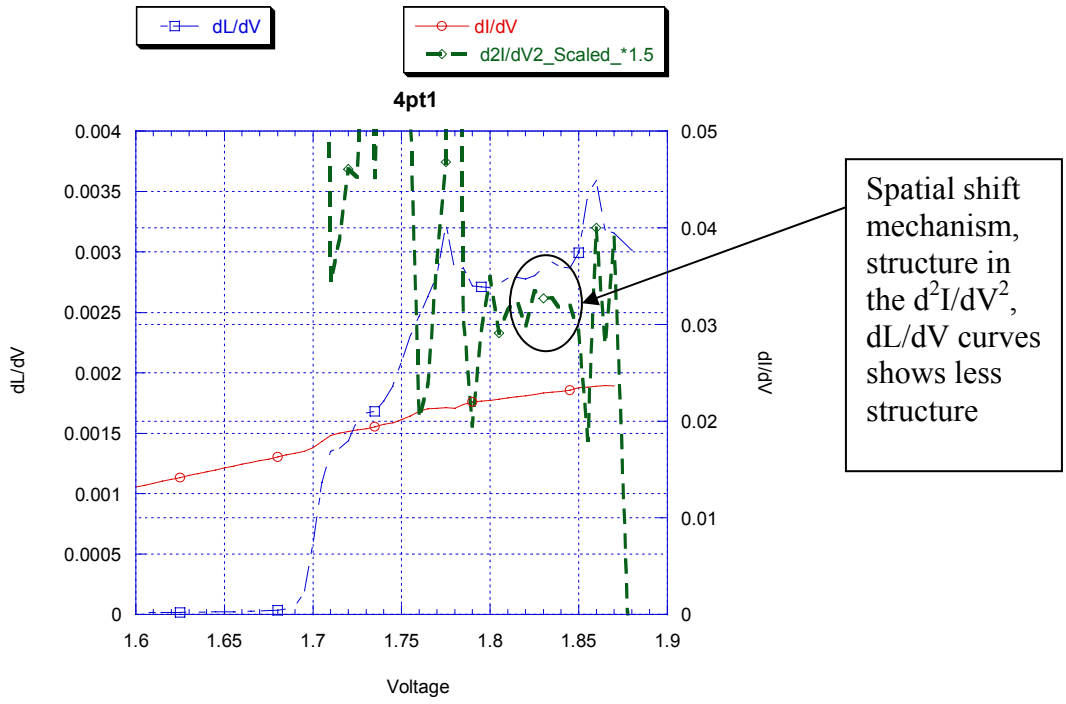

Figure 39. Spatial mode shift of the light output. Second derivative of current shows a large amount of structure while the dL/dV curve shows a region with less structure. One would also expect only minor variations in the light output since no new laser filaments evolve, only spatial shifting of the existing filaments.

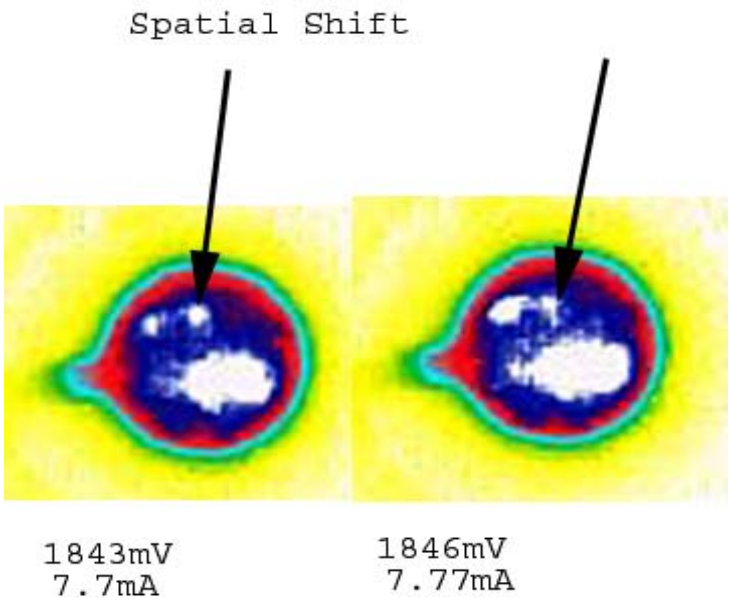

Figure 40 Optical image of a spatial shift, corresponding with the derivative structure displayed in Figure 39. One explanation for a spatial shift of a laser filament is that a new section of the active region provides a better (lower resistance) path to the current. This change in the preferred path of the current could be due to localized heating, current crowding, etc but the specific cause is not important at this point, only that the shift can happen.

The quasi-fermi levels must also be locked for the second mechanism to work. Laser action is already taking place, which justifies the quasi-fermi level locking. If the quasi-fermi levels are locked and the current finds a more favorable path, this creates opportunities for the laser filament to move to a new location or combine with an existing filament. When the current path (excess carriers) moves to a new portion of the active region not currently lasing, the filament appears to shift.

The third mechanism that may explain other variations of the derivative structure is a new filament starts to lase while another filament stops lasing. If a laser filament were to stop lasing and a new mode start at the same time then the derivative structure will change according to strength of the new or failing mode and the path of the current flow. The dL/dV curve may not show as sharp of a rise for this mechanism as for a new mode starting. A failing laser filament should have the opposite effect of a new laser

filament, where the light output efficiency goes down or flattens. This mechanism is much harder to find in the electrical derivative because of the relationship between rising and falling filaments. Depending on the strength of the new or failing filament the derivative may peak, drop, or flatten. In this case it is difficult to predict the exact movement of the derivative curves due to competing processes.

5. Chapter 5 – Analysis of Oxide Data and Comparison of Results

5.1. Overview

Using the L-V and I-V curves simple relationships between light and electrical signals were shown in chapter 3.1.2. More complex relations can also be observed when looking at the light and current derivative curves of these VCSELs (dL/dV, dI/dV, d^2I/dV^2). To better understand the correlations made between the light and current derivatives near-field images are investigated. The light derivatives and the near-field images are shown to be directly related and with the simple relationships between the light and current derivatives, the electrical signals can also be related to the optical observations.

Three mechanisms have been identified as the cause of the derivative structure found after threshold in these devices. These mechanisms are discussed in the following chapters.

5.2. Near Field Optical and Derivative Measurements in Oxide Defined VCSEL

Optical output patterns for a particular VCSEL are unique and reproducible for different test runs. The reproducibility of the output patterns reinforces the reproduced derivative structure for the VCSEL. If a different optical pattern were to occur during each test then we would expect the derivative structure to change from run to run also.

Given the reproducible results for both the derivative structure and optical mode patterns three distinct mechanisms can be observed. The first mechanism is laser action

or the start of a new mode in a particular portion of the active region. Laser threshold is the primary example of this mechanism. A new laser mode that starts shows a rapid rise in current and light for a small rise in voltage. The first derivative of light also displays a distinct rise in light output efficiency. In turn each additional laser mode that starts to lase should display a sharp rise in dL/dV and dI/dV with a corresponding peak in the d^2I/dV^2 curve. This can be seen in Figure 41 at threshold ~1620mV.

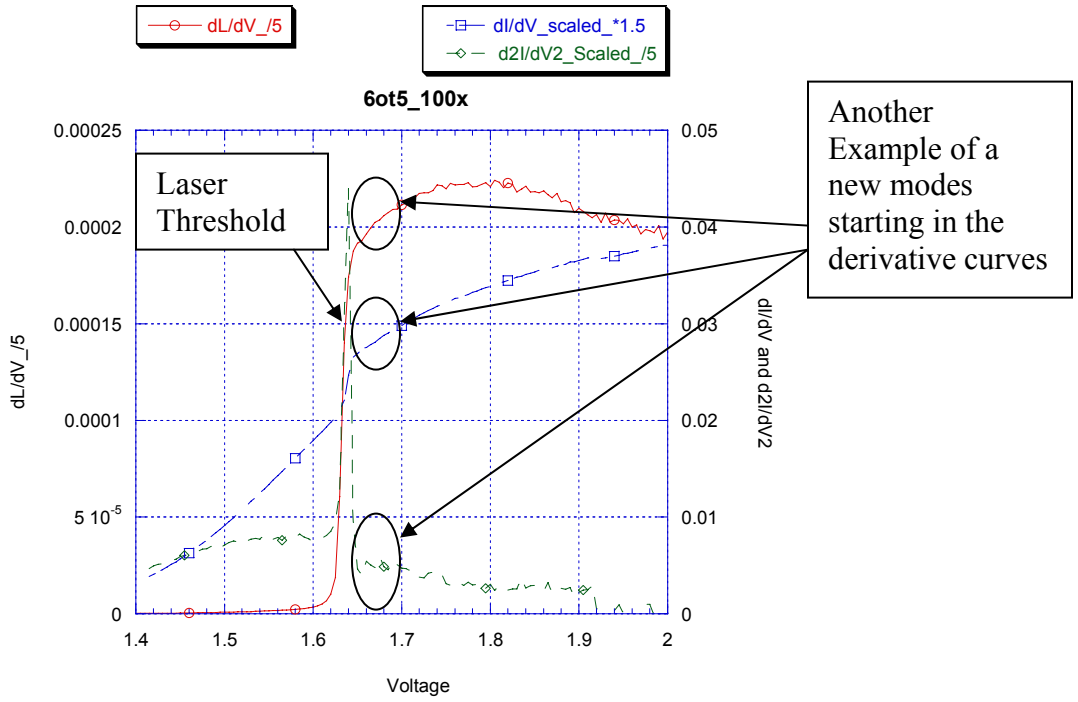

Figure 41 The first mechanism is seen at threshold where a new laser mode is formed. Note that at threshold there is a rapid rise in dI/dV, dL/dV, and a narrow peak in d^2I/dV^2.

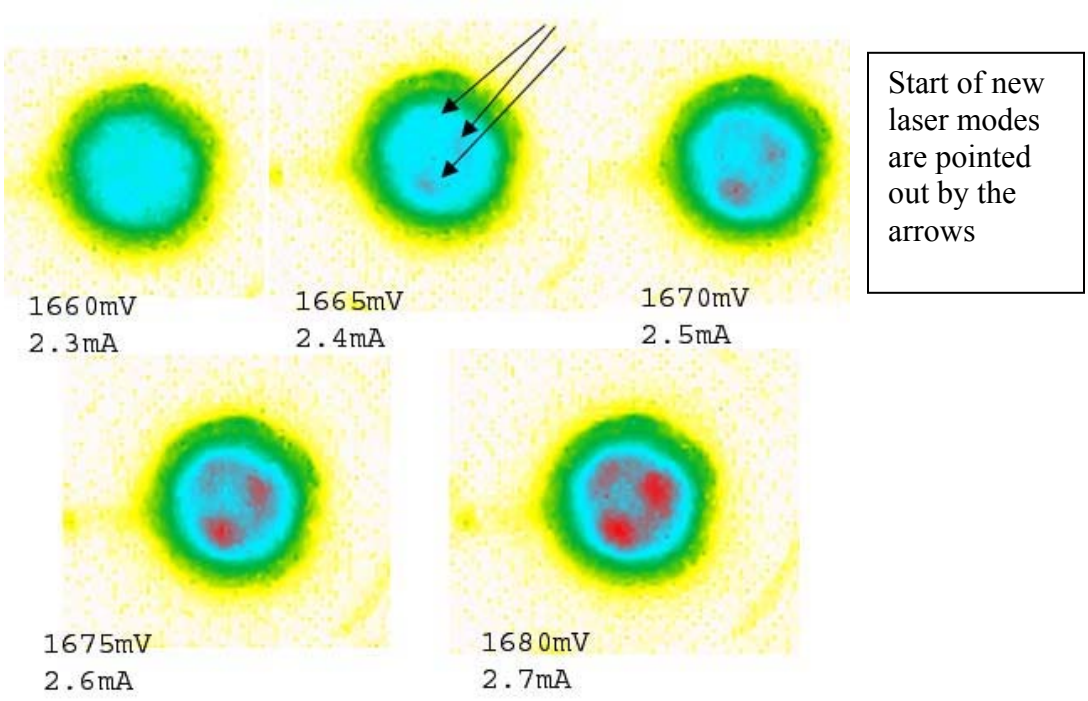

Figure 42 New mode starts at ~1660mV pointed out by the arrow. These modal patterns correspond with the derivative curves in Figure 41.

An example of a new laser mode starting above threshold is observed at ~1.660V in Figure 41. The corresponding modal patterns are shown in Figure 42 as a function of applied voltage. The location of the new mode is pointed out by the arrows in Figure 42. This mode starts to lase at ~1660mV. Prior work using narrow stripe geometry lasers has shown that the quasi Fermi levels lock (or saturate) after the onset of stimulated emission.[5] This mechanism is responsible for the rapid rise in the conductance, dI/dV, at threshold. It is best observed in homogeneous small geometry devices with minimal variation in the current distribution across the active region.[5]

Unfortunately VCSELs have a large emission aperture with a non uniform current distribution. Hence, to model the devices investigated, the active region is conceptually divided into an interconnected mesh of smaller individual laser diodes. These smaller

diodes can start to lase at different input voltages and have different geometries. An example of this model can be viewed in Figure 43.

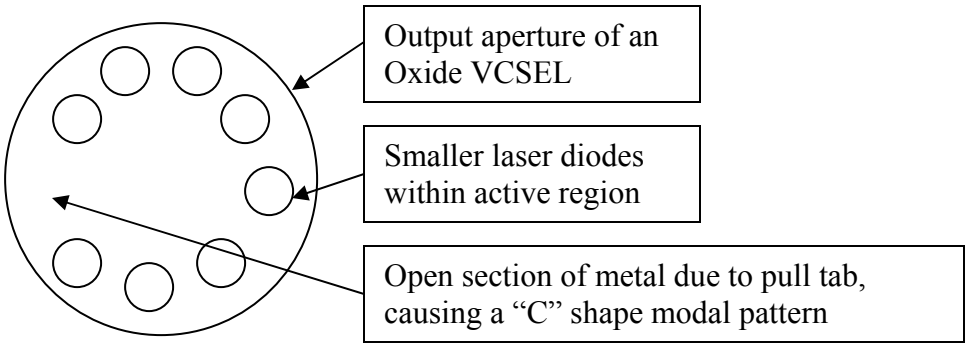

Figure 43 Representation of output aperture of an oxide VCSEL with a number of smaller laser modes inside the active region of the device. Note the modes form a "C" shape, this is due to a hole in the metal contact which causes little or no current to flow in the open portion of the "C" so no modes can start to lase.

At laser threshold a large portion of the active region is found to start lasing which corresponds to a sharp rise in all three derivative curves. The quasi-fermi levels are expected to lock for that particular portion of the active region. At higher drive voltages above threshold portions of the active region turn on and start laser action corresponding to the rapid rise in light and current derivative curves as seen in Figure 41 and Figure 42.

One explanation for a spatial shift of a laser mode is that a new section of the active region provides a better (lower resistance) path to the current. This change in the preferred path of the current could be due to localized heating, current crowding, etc but the specific cause is not important at this point, only that the shift can happen. Under the circumstances one would expect the conductivity to increase but not as rapidly as the core of a new mode developing. One would also expect only minor variations in the light output since no additional new laser modes evolve, only spatial shifting of the existing modes. These trends appear in the derivative measurements in the voltage range from ~1700mV to 1750mV in Figure 44. Based on Figure 44 a new mode appears to be

forming between 1700mV and 1740mV (sharp rise in d^2I/dV^2) but it never attains a strong narrow d^2I/dV^2 peak. Rather, as seen in Figure 45, the modes shift spatially about the active region while the optical derivative dL/dV remains almost constant as seen in Figure 44.

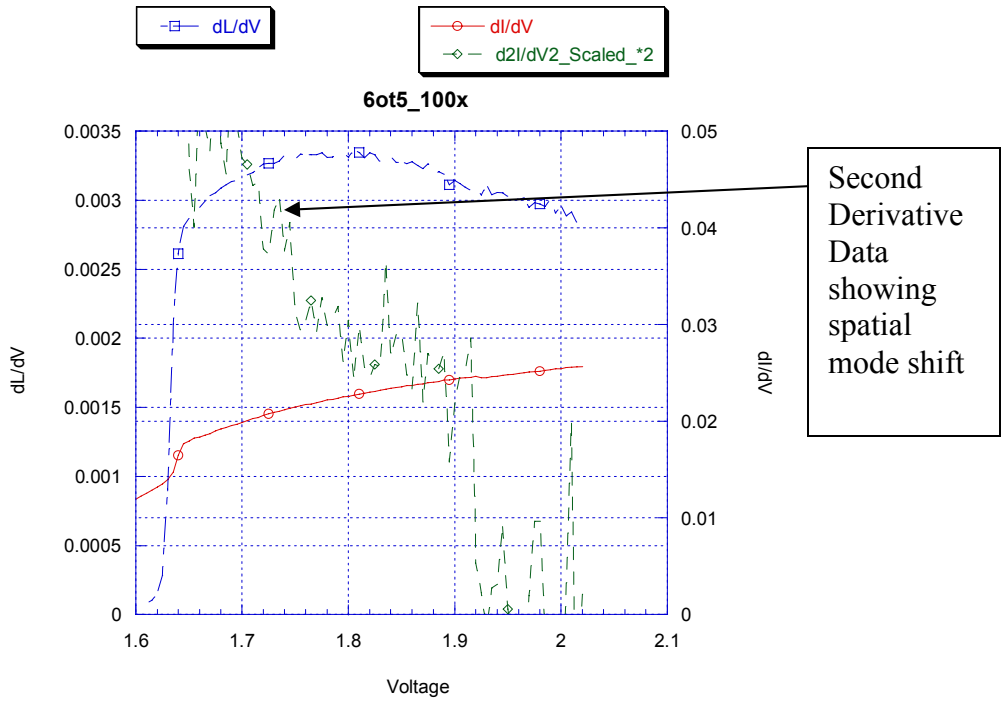

Figure 44 Spatial shift of the light output, second derivative of current shows a large amount of structure while the dL/dV curve shows a region with less structure. One would also expect only minor variations in the light output since no new laser modes evolve, only spatial shifting of the existing modes.

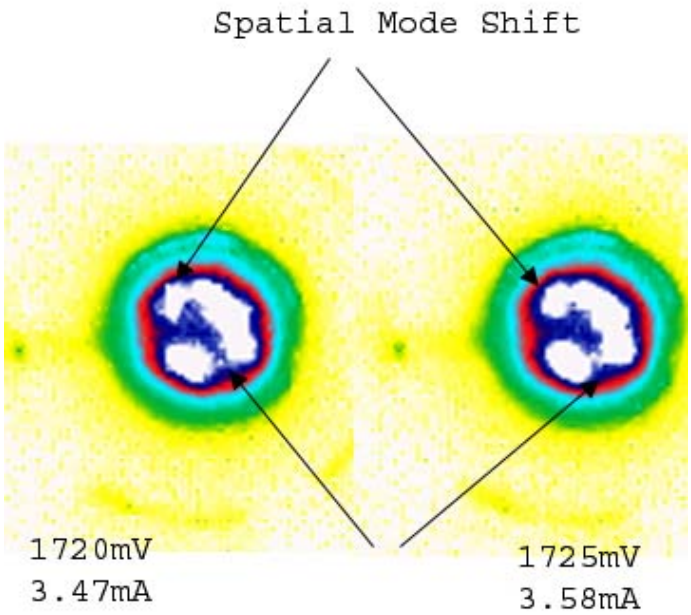

Figure 45. Optical image of a spatial shift, corresponding with the derivative structure displayed in Figure 44. One explanation for a spatial shift of a laser mode is that a new section of the active region provides a better (lower resistance) path to the current. This change in the preferred path of the current could be due to localized heating, current crowding, etc.

The quasi-fermi levels must also be locked for the second mechanism to work. Laser action is already taking place, which justifies the quasi-fermi level locking. If the quasi-fermi levels are locked and the current finds a more favorable path, this creates opportunities for the laser filament or mode to move to a new location or combine with an existing mode. When excess carriers move across a portion of the active region not currently lasing, the mode appears to shift.

The third mechanism happens in much the same way explained in chapter 4.2 however, this mechanism does not appear to be as prominent in the oxide VCSELs. The optical stability provided by the oxide layer overrides some of the shifting and electrical anomalies.

6. Chapter 6 – Summary and Conclusions, Future Work

6.1. Summary

Derivative spectroscopy has been used to better understand the inner workings of Vertical Cavity Surface Emitting Lasers. This laser structure has the emitting area perpendicular to the active region. Edge emitting lasers have been intensively investigated with many techniques including derivative spectroscopy. In contrast VCSELs are relatively new compared with edge emitting lasers, and hence have not been characterized as thoroughly as edge emitting structures. In this thesis derivative spectroscopy is used to investigate two types of commercially available Honeywell VCSELs, oxide confined VCSELs and proton bombarded VCSELs.

To understand a device as complicated as the VCSEL, measurements other than the standard I-V and P-I curves must be taken. For instance the first derivative of the I-V curve can be used to find series resistance that may cause roll-over of the current. Second derivative measurements can illuminate a process that is parasitic in nature and causes undesired optical patterns or mode shifts. The I-V and P-I curves are where this system of derivatives starts. Along with the derivative measurements optical observations help confirm the start of new modes or spatial mode shifts.

In order to use derivative spectroscopy along with the optical observations correlations between electrical and optical data had to be made. Simple relationships were found and explained for both devices in chapters 3.1.2 and 3.2.2. These simple relationships were used to help find other correlations between the second derivative of

current and the first derivative of light as seen in Figure 23 and Figure 31. The same correlations are found in both the oxide and proton confined VCSELs.

6.2. Comparison of the VCSESLs

We have identified three mechanisms that can be observed in both near-field optical patterns and the electrical and optical derivatives. The three mechanisms are: a new mode starts to lase; a spatial mode shift; and a new mode starts to lase while another mode dies. The relative importance of these three mechanisms is different in the proton and oxide defined VCSELs. Several reasons are provided as possible causes for the differences between the devices.

One significant difference between the oxide and proton defined VCSELs is the amount of lateral index step that defines the output aperture. The oxide layer provides much more optical confinement than the proton confinement. This may account for the difference in optical derivatives between the devices. Proton confined devices had much more optical derivative structure than the oxides as seen in Figure 36 and Figure 41. In the oxide VCSELs, the modes that start to lase after threshold seem to become more stable with more drive voltage. These modes become stronger and do not seem to have as many spatial shifts as the proton VCSEL modes. The oxide devices have more stable optical images which correspond to less derivative structure found in the oxide derivative data.

The optical emission pattern from the oxide defined devices appears to be dominated by the well defined allowed optical modes within the lateral cavity. In

contrast, the optical pattern in the proton defined devices appears to be dominated by the development of laser filaments rather than cavity modes. Another difference between the two laser structures is that the oxide VCSELs have a “C” shape. The metal contact that applies the input bias also has a “C” shape. Current flowing through the “C” shaped metal contact along with current crowding can produce the “C” shaped output pattern found in Figure 45. The reduced spatial mode shifting in the near-field optical output of the oxide devices may be due to the open portion of the metal contact which results in reduced current flow in the adjacent region. With insufficient current flow to that particular region no new mode or shifting can take place. The edge of the metal contact seems to have most all of the spatial regions occupied by a mode. Since modes already occupy those regions less mode shifting will occur. In contrast the “C” shape of the metal contact does not appear to help stabilize the proton VCSELs.

6.3. Mechanism Model

The three mechanisms have similar electrical characteristics due to the fact that all happen in the presence of quasi-fermi level locking. Modeling what is expected of the VCSEL will help to understand what may be happening within these devices. This model is based on spatially dependent quasi-fermi level locking. With the observations more complete models can be developed to include other mechanisms such as heating effects and gain saturation. An overview of what happens in each case can be viewed in Table 1.

Mechanism	What is expected*	What is observed
#1 New Mode Forms	dI/dV increases abruply; dL/dV increases abruptly and stays up > 0; d2I/dV2 peaks and stays > 0	dI/dV increases abruply; dL/dV increases and stays > 0 d2I/dV2 peaks and stays > 0
#2 Spatial Shift of Mode or Filament	dI/dV slight rise dL/dV stay > 0 but does not increases d2I/dV2 peak and stay > 0	dI/dV slight increase dL/dV slight increase d2I/dV2 multiple small peaks and valleys; stays > 0
#3 New Mode Forms and Another Mode Dies	dI/dV (**new mode strong**) increases abruptly; dI/dV (**new mode weak**) decreases slightly; dL/dV(**new mode strong**) increases and stays up > 0; dL/dV(**new mode weak**) decreases and stays > 0; d2I/dV2(**new mode strong**) increase to a peak and stays > 0; d2I/dV2(**new mode weak**) goes negative to a min then rises	dI/dV (**new mode strong**) increases abruptly; dI/dV (**new mode weak**) decreases slightly; dL/dV(**new mode strong**) increases and stays up > 0; dL/dV(**new mode weak**) decreases and stays > 0; d2I/dV2(**new mode strong**) increase to a peak and stays > 0; d2I/dV2(**new mode weak**) goes negative to a min then rises

* Based on simple model of spatially dependent quasi-fermi level locking

Table 1 Discusses what is expected and what is observed in the three mechanisms seen in the VCSELs.

6.4. Future Work

The following improvements to the experimental apparatus should be considered. To further investigate these VCSEL structures higher order derivatives of light (d^2L/dV^2) and current (d^3I/dV^3) would be helpful. The second derivative of the light should make it easier to find correlations between the optical characteristics and the electrical measurements. The third derivative of the current would help identify structure and serve as a check of noise sources in the second derivative.

Another potential improvement would be to modulate the current rather than the voltage. The exponential dependence of the current on the voltage produces large changes in the optical output for very small changes in voltage. Modulating the current would simplify the identification of narrow peaks and stretch out the rapid variations of the derivative signals. The down side of using a current source is that new setup and testing protocols need to be developed to ensure that the open circuit voltage of the current source does not damage the laser diode.

The camera setup that takes images of the near-field can be improved in multiple ways. The amount of optical attenuation used in the experiment now only allows images to be taken up to 1900mV (~ 8mA). More attenuation would allow images to be take of the higher input biases without adjusting the gain on the camera. The resolution of the images can also be improved by replacing the camera with a better camera.

The diagrams seen in Figure 38 and Figure 43 illustrate that the VCSELs can be modeled as many other smaller devices within the active region of these devices. A mathematical model of where each of the smaller devices are located and how the smaller

devices work in relation to each other would help to determine what the quasi-fermi levels are doing for a given input bias.

Temperature dependence may be a cause of the optical shifting seen in the devices. Heating effects may cause the current to flow in different portions of the active region allowing laser action in a particular portion and not in another. This heating effect might be controlled by better heat sinks. The devices dissipate heat through two wire leads out of the device and heat loss by air cooling. Another cause of the shifting may be attributed to gain saturation. If an area of gain is saturated and another area is not being used then a filament or mode may slide over to use the unsaturated gain.

REFERENCES

[1] H. Soda, K. Iga, C. Kitahara & Y. Suematsu, "GaIn AsP / InP Surface Emitting Injection Lasers," Jpn. J. Appl. Phys., 18, 12, p2329, 1979

[2] T. L. Paoli, and J. F. Svacek, "Derivative measurement by frequency mixing," Rev. Sci. Instrum., vol. 47, pp. 1015-1019, Sept. 1976.

[3] H. W. Korb and N. Holonyak, Jr., "Measurement system for derivative studies," Rev. Sci. Instrum. 43, pp. 90-94 (Jan. 1972).

[4] R. W. Dixon, "Derivative measurements of light-current-voltage characteristics of (AlGa)As double-heterostructure lasers," Bell System Tech. J. 55, pp. 973-980 (Sept. 1976).

[5] P. A. Barnes and T. L. Paoli, "Derivative measurements of the current-voltage characteristics of double-heterostructure injection lasers," IEEE J. Quantum Electronics. QE-12, pp. 633-639 (Oct. 1976).

[6] W. B. Joyce and R. W. Dixon, "Fundamental and harmonic response voltages of a sinusoidally current-modulated ideal semiconductor laser," J. Appl. Phys. 47, pp. 3510-3513 (Aug. 1976).

[7] T. L. Paoli, "Optical derivative measurements of the electrical parameters for a junction diode," Appl. Phys. Lett. 35, pp. 339-341 (Aug. 1979).

[8] T. L. Paoli, "Theoretical Derivatives of the electrical characteristics of a junction laser operated in the vicinity of threshold," IEEE J. Quantum Electronics QE-14, pp. 62-68 (Jan. 1978).

[9] T. L. Paoli, "Nonlinearities in the emission characteristics of stripe-geometry (AlGa)As double-heterostructure junction lasers," IEEE J. Quantum Electronics QE-12, pp. 770-776 (Dec. 1976).

[10] T. L. Paoli, "Observation of second derivatives of the electrical characteristics of double-heterostructure junction lasers," Transactions on Electronic Devices ED-23, pp. 1333-1336 (Dec. 1976).

[11] T. L. Paoli, "Determination of the lasing threshold in stripe-geometry double-heterostructure junction lasers," Appl. Phys. Lett. 29, pp. 673-675 (Nov. 1976).

[12] A. Ramaswamy, J. P. van der Ziel, J. R. Biard, R. Johnson, and J. A. Tatum, "Electrical characteristics of proton-implanted vertical-cavity surface-emitting lasers," IEEE J. Quantum Electronics 34, pp. 2233-2240 (Nov. 1998).

[13] J. Li, J. F. Seurin, S. L. Chuang, K. D. Choquette, K. M. Geib, and H. Q. Hou, "Correlation of electrical and optical characteristics of selectively oxidized vertical-cavity surface-emitting lasers," Appl. Phys. Lett. 70, pp. 1799-1801 (Apr. 1997).

[14] J. Kim, J. Boyd, H. Jackson, and K Choquette, "Near-field spectroscopy of selectively oxidized vertical cavity surface emitting lasers," Appl. Phys. Lett. vol. 76, Num. 5, pp. 526-528 (Jan. 2000).

[15] Y. Lee, J. Jewell, A. Scherer, S. McCall, J. Harbison, and L. Florez, "Room-temp. Continuous-wave vertical cavity single quantum well microlaser diodes," Electon. Lett., 25, 20, p.1377, 1989

[16] N. Holonyak Jr., "The Semiconductor Laser: A Thirty-Five Year Perspective", Proc. Of IEEE, vol. 85, No. 40, Nov. 1997

[17] J. Pankove, "Optical Processes in Semiconductors", Dover Pub., New York, 1975

[18] G. P. Agrawal, N. K. Dutta, "Semiconductor Lasers, 2nd ed.", Van Nostrand Reinhold, New York, 1993

[19] T. E. Sale, "Vertical Cavity Surface Emitting Laser", Wiley & Sons Inc., New York, 1995

[20] B. Hawkins, R. Hawthorne, J. Guenter, J. Tatum, J. R. Biard, "Reliability of Various Size Oxide Aperature VCSELs", 2002; Honeywell International 830 E. Arapaho Road, Richardson, Texas 75081